

Graphene-based anti-corrosive coating on steel for reinforced concrete infrastructure applications: Challenges and Potential

Tanvir Qureshi ^{a,b,c}, Guorui Wang ^{a,d}, Sankha Mukherjee ^{a,e,f}, Md Akibul Islam ^{a,d}, Tobin Filleter ^{a,d}, Chandra V. Singh ^{a,e} and Daman K. Panesar ^{a,b,*}

^a UofT Centre for 2D Materials, University of Toronto, Canada

^b Department of Civil and Mineral Engineering, University of Toronto, Canada

^c Department of Geography & Environmental Management, UWE Bristol, UK

^d Department of Mechanical & Industrial Engineering, University of Toronto, Canada

^e Department of Materials Science & Engineering, University of Toronto, Canada

^f Department of Metallurgical and Materials Engineering, Indian Institute of Technology Kharagpur, India

* Corresponding author: D.K. Panesar (d.panesar@utoronto.ca).

Abstract

Steel corrosion has been a major perpetual issue of concern for durability and structural integrity of steel and reinforced concrete infrastructure. Polymeric, zinc-galvanic and chromate conversion coatings are commonly applied to protect typical steel materials such as structural steel, reinforcing steel bar (rebar), mild steel and light gauge steel used in infrastructure. Yet, due to physical integrity, long-term performance and environmental concerns, their applications have been limited. In recent years, graphene has garnered considerable attention in the field of anti-corrosive coatings and substantial progress has been achieved in the development of particular graphene-based monolithic (single/few-layer graphene and graphene oxides) as well as laminate and nanocomposite coatings. Despite considerable efforts dedicated towards fundamental research, the laboratory to industry transition of graphene-based anticorrosion coatings remains challenging. To this end, this report reviews the state-of-the-art on graphene-based coating technology with application to steel surfaces and discusses, both, experimental studies and theoretical aspects. Specifically, this review presents (i) production of different forms of graphene-based materials and the coating process; (ii) corrosion resistance and anti-corrosive coating performance of graphene-coated steel materials, (iii) key potential areas and challenges pertaining to the application of graphene-based coating to structural steel and rebar; and (iv) potential future directions towards corrosion protection and smart coatings.

Keywords: graphene, laminate, nanocomposite, coating steel, anti-corrosion.

Table of contents

| |
|---|
| 1. Introduction |
| 2. Graphene-based anti-corrosive coating |
| 2.1. Graphene-based monolithic coating |
| 2.1.1 Corrosion protection mechanism |
| 2.1.2 Preparation/coating methods |
| 2.1.3 Anti-corrosion performance |
| 2.2. Graphene-based laminate coating |
| 2.2.1 Corrosion protection mechanism |
| 2.2.2 Preparation/coating methods |
| 2.2.3 Anti-corrosion performance |
| 2.3. Graphene-based nanocomposite coating |
| 2.3.1 Corrosion protection mechanism |
| 2.3.2 Preparation/coating methods |

| | |
|----|--|
| 46 | 2.3.3 Anti-corrosion performance |
| 47 | 3. Challenges and potential of graphene-based anti-corrosive coating in structural steel and rebar for |
| 48 | infrastructure application |
| 49 | 3.1 Long-term stability |
| 50 | 3.2 Scalability |
| 51 | 3.3 Cost-effectiveness |
| 52 | 3.4 Quality |
| 53 | 3.5 Environmental sustainability |
| 54 | 4. Future prospects |
| 55 | 5. Conclusions |
| 56 | Acknowledgement |
| 57 | References |
| 58 | |

59 **1. Introduction**

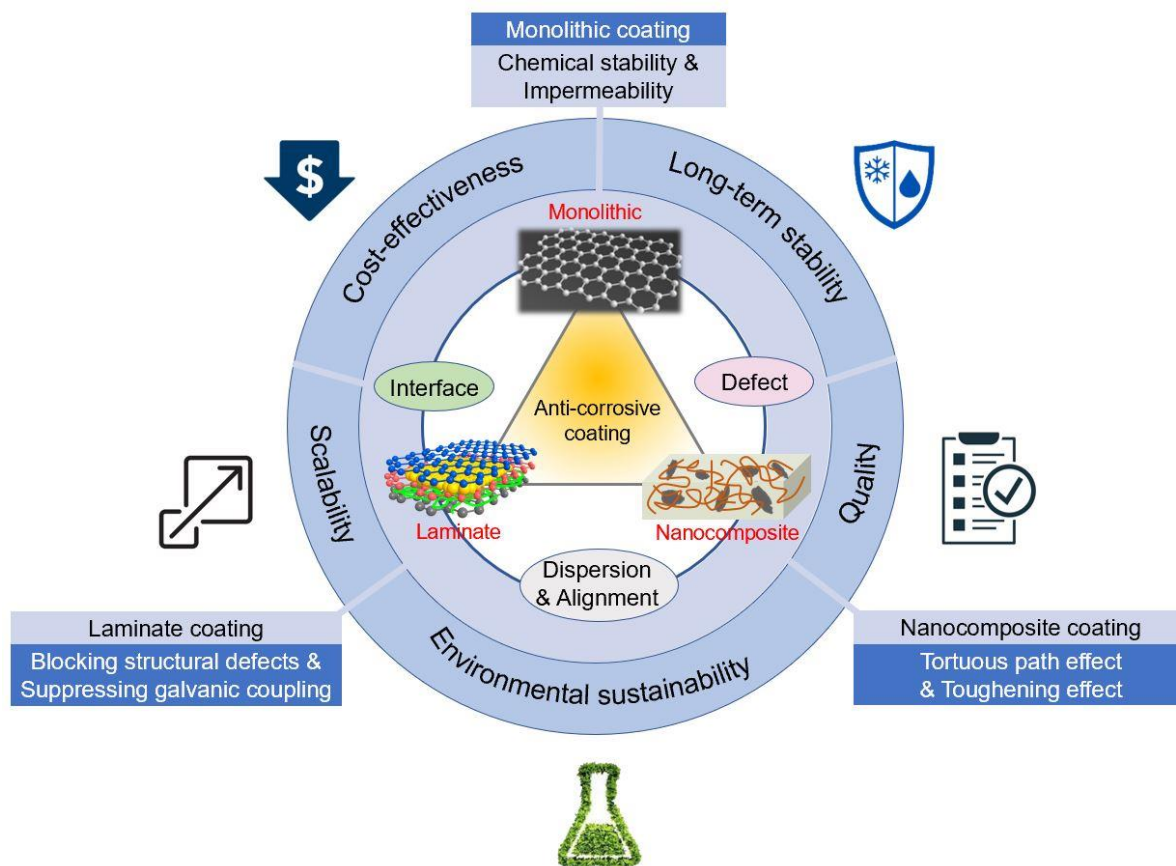
60 Steel materials have wide applications in steel and reinforced concrete infrastructure development.
61 Carbon steel (0.12-2.00% carbon) and alloy steel (carbon steel alloying other elements) grades
62 commonly account for the production of structural steel, steel reinforcing rebar, mild steel, and light
63 gauge steel. Structural steel with different shapes and hollow structural sections is extensively used as
64 structural beams and columns in steel structure construction. Steel rebar typically made with carbon
65 steel serves as a reinforcing agent in reinforced concrete structure construction. Over time, both the
66 structural steel and rebar are susceptible to extensive corrosion when they are exposed to the corrosive
67 environment such as in marine conditions or de-icing salt exposure. For example, corrosion of steel
68 rebar can lead to the cracking of concrete, spalling, and staining of the reinforced concrete
69 infrastructure, which is a major concern for the sustainability, safety, durability and economic
70 implications pertaining to civil infrastructure [1]. In reality, corrosion of metals globally accounts for
71 US\$2.5 trillion annually [2], where a significant part of this cost is associated to the durability of steel
72 and reinforced concrete structure. In the USA, the average direct cost of corrosion protection for
73 highway concrete bridges in 2002 was estimated \$8.3 billion annually which expected to be much
74 higher in 2021 considering inflation [3].

75 Corrosion of steel rebar is a major durability concern in reinforced concrete materials systems. Steel
76 rebar embedded in the concrete matrix are typically protected by a passive oxide layer developed in the
77 interface due to a relatively high pH of concrete [4]. There are two common steel rebar corrosion
78 mechanisms in concrete. One is the penetration of chloride ions through porous concrete such as in
79 marine environment or sourced from de-icing salt which can cause pitting corrosion [5], and the other
80 is the carbonation of concrete when atmospheric CO₂ reacts with portlandite of concrete at the presence
81 of water and reduces the pH of concrete from approximately 13 to 9, which diminishes the protective
82 passive layer of steel rebar [6]. Therefore, the effects of increasing chloride concentration to meet or
83 exceed the critical chloride concentration and/or the reduction in pH value of the concrete pore solution,
84 leads to the initiation of corrosion of steel rebar surface [7]. The corrosion of steel results in the loss of
85 original cross-section, as well as up to six times the volume expansion causing debonding of rebar from
86 concrete, ultimately resulting a failure of the composite material system and in turn affecting the
87 integrity of the structure. Application of an anti-corrosive coating to structural steel and rebar embedded
88 in concrete, can be an effective solution. Barrier protective coating systems, such as polymers (e.g.,
89 epoxy layer, paints), metal (e.g., iron-zinc alloy/ galvanizing), enamel (e.g., porcelain/vitreous made by
90 fusing powdered glass) and nanoparticle-based composites (e.g., polyurethane-nano-SiO₂, epoxy with
91 nano-SiO₂ or Fe₂O₃ or Zn, alkyd resin with nano-ZnO or nano-Al₂O₃) are typically used to restrict
92 contact of moisture and oxygen to the surface of the steel [8–15]. However, these conventional coatings

93 have their respective limitations in performance and service life. Some common drawbacks include:
94 chemical reactions in fresh concrete with galvanized bar, weak bond between steel and surrounding
95 concrete with epoxy-coated bar, and brittleness of enamel coating [16]. These can result in abrasion of
96 coating layer during transportation and construction handling, defects in the coating during fabrication,
97 and lead to pitting corrosion. Polymer coatings are susceptible to high-temperature degradation and
98 suffer from their inherent porosity. Furthermore, the use of thick coatings may disrupt the functionality
99 (e.g. electrical and thermal conductivity) and component dimensionality of target metals [17,18]. Other
100 approaches for carbon steel and alloy steel corrosion prevention are the use of cathodic and anodic
101 protections, and stainless steel or glass fibre reinforced polymer (GFRP) as a costly alternatives have
102 limitations in terms of bending, ductility, cutting and joining required for reinforced concrete
103 infrastructure [19].

104 In comparison to traditional approaches, graphene has become a potentially important candidate for
105 surface coatings against corrosion owing to its chemically inert nature and impermeability to gases and
106 liquids, and is an emerging field of research [20]. As the strongest known material, graphene possesses
107 an ultrahigh fracture strength (~ 100 GPa) [21], and ultrahigh fatigue life ($>10^9$ cycles) which can benefit
108 a structure's integrity under severe and complex loading conditions [22]. Its superlubricity and ultralow
109 friction further enables the graphene-based coating to exhibit desirable properties including, high wear
110 and scratch resistance [23,24]. Moreover, other properties such as thermal conductivity (up to 5000
111 $\text{Jm}^{-1}\text{K}^{-1}\text{s}^{-1}$) and functionalization potential [25–29], are also crucial for retaining the functional
112 properties of the metal beneath the coating. In addition, due to the atomic thickness (~ 0.34 nm),
113 graphene considerably reduces the volume of coating material, compared to other more traditional
114 coating materials. In light of the diversification of commercial barrier coatings that are application-
115 specific, graphene can also be integrated with other barrier materials that complement each other (e.g.
116 ceramic and polymer) to construct a laminate coating and a composite coating. In this scenario,
117 graphene provides the barrier function, meanwhile ceramic and polymer offer other functionalities
118 needed for an effective and long-lasting protection.

119 Despite substantial progress achieved in the fundamental research of graphene-based anti-corrosive
120 coatings, the path from laboratory to industry poses daunting challenges. Some of the key significant
121 challenges at stake for industrialization of graphene-based anti-corrosive coating include the quality
122 control of graphene materials, scalable deposition of graphene-based coatings on substrates, long-
123 lasting corrosion protection strategies, optimization of manufacturability to account for cost and
124 reliability, and the corresponding environmental impacts. In contrast to review articles [30–36], that
125 provided an overview of the scientific state-of-the-art and relevant technical details, in this review, we
126 present a full account of challenges and potential of graphene-based coatings for anti-corrosion
127 applications on structural steel and rebars, with a special emphasis towards their industrialization and
128 commercialization. As outlined in Fig. 1, Section 2 will present three forms of graphene namely,
129 monolithic, laminate, and nanocomposite coatings. For each type of graphene-based coating, the
130 mechanisms which rely on the physics and chemistry behind the protective efficiency (e.g.
131 impermeability, structural integrity, etc.), the preparation of coating materials and coating methods,
132 anti-corrosion properties, common failure modes and mechanisms (e.g. defect, interface, etc.), and
133 performance optimization measures are presented. Upon synthesis and critical review of the three
134 coating options in terms of different factors (e.g. long-term stability, cost, scalability, quality and
135 environmental sustainability), a recommended approach is presented for coating steel with application
136 to infrastructure.



137

138 **Fig. 1** Overview of graphene-based anti-corrosive coatings, including graphene-based monolithic, laminate and
 139 nanocomposite coating, showing coexistence of challenges and opportunities.

140

141

142 2. Graphene-based anti-corrosive coating

143 The development of graphene-based anti-corrosive coating for steel surfaces have progressed along
 144 three avenues: (i) graphene-based monolithic coating, (ii) graphene-based laminate coating, and (iii)
 145 graphene-based nanocomposite coating. For each coating category, the key advancements related to
 146 corrosion resistance and the corresponding synthesis and coating processes types based on literature
 147 reports are summarized in Table 1. In this section, a brief introduction of the three coating systems will
 148 be given, including corrosion protection mechanisms, preparation/coating methods and anti-corrosion
 149 performance.

150

151

152 **Table 1.** Materials processing and coating techniques and corrosion performances on the graphene-based anticorrosive coating on iron/steel surface.

| Graphene-based monolithic coating | | | | | | |
|---|------|-------------------------------|---------------------------------|---|--|------|
| Materials synthesis and coating process | Year | Coating thickness | Corrosion performance | | | Ref. |
| | | | Testing environment | Resistance | Rate | |
| CVD grown graphene on metals (Cu, Pt, Ni, Co, Fe) at low temperature (650 °C) | 2015 | Single layer graphene | Air exposure | Cu, Pt: weakly interacting, ready access for oxidizing Ni, Co: Strongly interacting, passivating oxide Fe: Strongly passivating, non-passivating oxide so initially slow but accelerate in long term exposure | No data reported | [37] |
| CVD grown graphene on Ni-buffered SS at 700-900 °C (Ni/SUS304) | 2015 | Single to multilayer graphene | 3.5 wt% NaCl solution | ICR increases after 20 scans in Graphene, Ni/SUS304: 30 → 36 mΩ cm ² SUS304: 158 → 560 mΩ cm ² | Corrosion resistance, I _{current} (A·cm ⁻²) after 20 scans in: SUS304: 1.49 × 10 ⁻⁷ → 7.41 × 10 ⁻⁶ Graphene-Ni/SUS304: 1.61 × 10 ⁻⁷ → 1.63 × 10 ⁻⁷ (~45 times lower than SUS304); | [38] |
| CVD grown graphene on SS at low temperature (400°C) | 2016 | Single or few-layer graphene | 5% wt.% sea salt solution | Stable and long-lasting anticorrosion after long-term immersion | Corrosion rate lowers up to 10 times, Bare steel: 1.75 × 10 ⁻¹³ m.s ⁻¹ Coated steel: 2.02 × 10 ⁻¹⁴ m.s ⁻¹ (~9 times lower than bare steel) | [39] |
| Graphene grown on carbon steel by laser processing | 2015 | Multilayer graphene | 3.5% wt.% NaCl aqueous solution | Up to ~1900 Ω cm ² , almost 7 times that of original steel (270.7 Ω cm ²). | 0.05 mm/year, much lesser than that of the stainless steel (0.09 mm/year) | [40] |
| rGO ink coated Fe sample | 2013 | 1.2–1.4 nm | 1% wt.% NaCl solution | Coating resistance increases from 17 Ωcm ² for bare Fe to 766 Ω cm ² for graphene ink/Fe | No data reported | [41] |
| rGO nanosheets deposited on carbon steel by | 2016 | / | 3.5% NaCl aqueous solution | Corrosion current density (J _{corr}): 69.2 μA cm ⁻² for bare carbon steel | 0.804 mm/year for bare carbon steel surface → 0.354 mm/year for rGO coated carbon steel | [42] |

| electrochemical deposition | | | | surface $\rightarrow 30.5 \mu\text{A cm}^{-2}$ for rGO coated carbon steel | | |
|---|------|-----------------------|---|---|--|--------------|
| Electrophoretic deposition of GO onto carbon steel | 2017 | Less than 10 nm | 3.5% wt.% NaCl aqueous solution | Corrosion current density: $11.83 \pm 0.86 \text{ mA cm}^{-2}$ for uncoated carbon steel $\rightarrow 4.14 \pm 0.64 \text{ mA cm}^{-2}$ for GO coated carbon steel | Reduce up to three times the corrosion rate of carbon steel | [43] |
| GO drop casting onto carbon steel rebar | 2021 | Several layer of GO | Concrete pore solution with 3.0 % wt.% NaCl | GO coating increases the resistance to $4150.47 \Omega \text{ cm}^2$ from $294.47 \Omega \text{ cm}^2$ for uncoated steel | Corrosion rate decreases in GO coated steel to 0.0089 mm/year from 0.85 mm/year in uncoated | [44] |
| Graphene-based laminate coating | | | | | | |
| Materials synthesis and coating process | Year | Coating thickness | Corrosion performance | | | Ref. |
| | | | Testing environment | Resistance | Rate | |
| $\text{Al}_2\text{O}_3/\text{TiO}_2/\text{rGO}$ by ALD on SS | 2016 | $\leq 200 \text{ nm}$ | 3.5% wt.% NaCl aqueous solution | $3.8 \times 10^6 \Omega \text{ cm}^2$ for bare SS $\rightarrow 4 \times 10^7 \Omega \text{ cm}^2$ for SS/rGO/ceramic laminate | No data reported | [45] [46] |
| CVD graphene/PVB hybrid films by spin coating-assisted layer-by-layer assembly on AA | 2014 | 4–5 μm | APS copper etchant | Corrosion current density: 4×10^{-5} – $4 \times 10^{-7} \text{ A cm}^{-2}$ for bare AA $\rightarrow 10^{-10} \text{ A cm}^{-2}$ for CVD graphene/PVB laminate coated AA | 4 $\mu\text{m/year}$ for bare AA $\rightarrow <2 \text{ nm/year}$ for AA/CVD graphene/PVB laminate | [47] |
| hBN/MoS ₂ /PVA drop cast on SS | 2013 | 5 μm | 3.5% wt.% of API salt aqueous solution | Corrosion current density: $6.46 \times 10^{-6} \text{ A cm}^{-2}$ for MoS ₂ coated SS $\rightarrow 4.50 \times 10^{-6} \text{ A cm}^{-2}$ for hBN/MoS ₂ laminate coated SS | No data reported | [48] |
| Graphene-based nanocomposite coating | | | | | | |
| Materials synthesis and coating process | Year | Coating thickness | Corrosion performance | | | Ref. |
| | | | Testing environment | Resistance | Rate | |
| 0.1-0.3 wt% GO in WPU dispersion, solution blending (PVA, Zinc oxide, CB) and dipping of MS | 2015 | 15–20 μm | 3.5% wt.% NaCl solution | Corrosion resistance: Rct–0.3% PGZ and PCZ = 34.21 and 27.08 $\text{k}\Omega \text{ cm}^2$ Overall PVA anchored GO/ZnO > CB/ZnO | 0.3% PGZ and PCZ = 56.85 and 10.37 $\text{k}\Omega \text{ cm}^2$ Corrosion rate of MS/WPU/0.3% PGZ and PCZ are almost 147 and 31 times lower than bare MS | [19] |

| | | | | | | |
|--|------|---|--|--|---|------|
| Graphene (high shear mixing + bath sonication), functionalized with APTES in water and applied by a bar applicator | 2015 | 4 μm , Dry film (30 \pm 5 μm) | 3.5% wt.% NaCl solution (pH 5.5 at 25 $^{\circ}\text{C}$) | Corrosion resistance ($R_{ct}+R_f$): Mild Steel = 550 $\text{k}\Omega \text{ cm}^2$, Chromate pre-treatment+Primer = $1.6 \times 10^6 \text{ k}\Omega \text{ cm}^2$; Graphite+Primer = $2.4 \times 10^5 \text{ k}\Omega \text{ cm}^2$; Functionalized graphene +Primer = $2.8 \times 10^6 \text{ k}\Omega \text{ cm}^2$ | Corrosion rate (mils penetration per year): Mild Steel = 30.386, Chromate pre-treatment+Primer = 0.087; Graphite+Primer = 1.732; Functionalized graphene +Primer = 0.015 (~2026 times lower than MS), | [49] |
| Composite mixed (wt%): APTES: 39.96-38; Water: 59.94-57; Graphene: 0.1-5. Coating was applied on MS by bar applicator and heat treated at 200 $^{\circ}\text{C}$ | 2017 | 3- μm dry film; 20 μm (wet film thickness) | 3.5 wt.% NaCl solution (freely exposed to air, pH 5.5 at 25 $^{\circ}\text{C}$) | The amount of water absorbed at saturation decreases with increasing graphene concentration up to 5% loading (74% reduction at 288 hours exposure) compared to APTES coated MS | EIS measurement in coated MS surface: APTES coating: 288 h severely damaged 5% graphene composite coating: far less damage even after 480 h of exposure. | [50] |
| GO, amino-terminated IL, epoxy composite using a grafting reaction (Q235) coated by a bar coater on Steel | 2018 | 30 \pm 2 μm | 3.5 wt.% NaCl aqueous solution | Salt spray test on steel: Pure epoxy and the epoxy 0.5 wt% rGO coating showed corrosion after 100 h, IL-GO composite coating was relatively clean after 300 h | Corrosion current changes: Epoxy-coated: 3.10 (1h) \rightarrow 4.75 $\mu\text{A} \cdot \text{cm}^{-2}$ (30h) IL-GO-coated: 2.20 $\mu\text{A} \cdot \text{cm}^{-2}$ (30 h) | [51] |
| GO synthesised heating <i>Aeschynomene aspera</i> plant at 1600 $^{\circ}\text{C}$ in an argon atmosphere; Cup-milling GO and sunflower oil (10 min), dip-coating on CR steel, and curing at 350 $^{\circ}\text{C}$ for 10 min at atmosphere | 2015 | 0.8 μm | 3.5 wt.% NaCl aqueous solution | Salt spray test: Red rusting in RC steel, GO ink coated: 100 h Oil coated: 24 h Bare (no coating): 6 h | Corrosion rate (mm/year) in CR steel: GO ink coated: 0.0000075 (10,000 times lower than bare steel) Oil coated: 0.01159 Bare (no coating): 0.1069 | [52] |
| rGO from secretion products of insect, <i>Laccifer Lacca</i> then PT: rGO dip coating heated at 710 $^{\circ}\text{C}$ for 24 h, and dip | 2018 | | 3.5 wt% NaCl aqueous solution at pH 7.3 and at room temperature (20 \pm 2 $^{\circ}\text{C}$) | EIS coating polarisation resistance, R_p : Bare: 0.99 $\text{k}\Omega \text{ cm}^2$ rGO coated: 0.62 $\text{k}\Omega \text{ cm}^2$ SO coated: 1.78 $\text{k}\Omega \text{ cm}^2$ | Corrosion rate (mm/year) in CR steel: Bare: 0.17958 rGO coated: 0.18922 SO coated: 0.03994 | [53] |

| | | | | | | |
|---|------|---|--------------------------------|---|---|------|
| coated CR steel in sunflower oil at 350 °C for 10 min | | | | PT coated: 823.2 kΩ cm ² | PT coated: 0.000017 (10,000 times lower than bare steel) | |
| Exfoliation and functionalization of graphite with ABA in PPA/P ₂ O ₅ then polyaniline/graphene 0.5 wt.%) composites (PAGCs) grafted on steel | 2012 | 29 μm | 3.5 wt.% NaCl aqueous solution | EIS, polarisation resistance, R _p : Bare: 2.48 kΩ cm ² PAGCs coated: 135.22 kΩ cm ² Protection efficiency (P _{Tahmina} %): Bare: None PAGCs coated: 53.49 PAGCs reduces water permeability 10 times than bare steel | Corrosion rate (mm/year) in CR steel: Bare: 0.1722 PAGCs coated: 0.0044 (39 times lower than bare steel) | [54] |
| Hydrophobic epoxy graphene composite (HEGC) mixed using three-roll mill and CR steel coated using a nanocasting technique | 2014 | Epoxy: 110 μm HE: 110 μm HEGC: 115 μm | 3.5 wt.% NaCl aqueous solution | EIS, polarisation resistance, R _p : Bare: 2.94 kΩ cm ² Epoxy: 25.46 kΩ cm ² HE: 37.87 kΩ cm ² HEGC: 442.00 kΩ cm ² | Corrosion rate (mm/year) in CR steel: Bare: 0.1648 Epoxy: 0.0254 HE: 0.0089 HEGC: 0.0023 (72, 11 and 4 times lower than bare, Epoxy and HE coating, respectively) | [55] |
| Poly (EVOH)-BA-GO compounds mixed using stirring and ultrasonication then spray coated on SS | 2018 | 21 ± 1 μm | 3.5 wt.% NaCl aqueous solution | EIS, polarisation resistance: Bare SS: 11 kΩ cm ² EVOH: 300 kΩ cm ² EVOH-BA-GO: 610 kΩ cm ² | Corrosion rate (mm/year): Bare SS: 0.2540 EVOH: 0.0247 EVOH-BA-GO: 0.0034 (~75 times lower than bare SS) | [56] |
| GO, rGO, MWCNT mixed to two-part epoxy resin painted with brush | 2022 | 270 ± 40 μm | Concrete from OPC | EIS corrosion current (90 days): Bare: 0.22A (29d); PE: 0.1 A rGO/CNT: 0.04A; GO/CNT: No | Mass loss in rebar: Bare: 24.5%; PE: 11.3% rGO/CNT: 8.6%; GO/CNT: 0.45% | [57] |

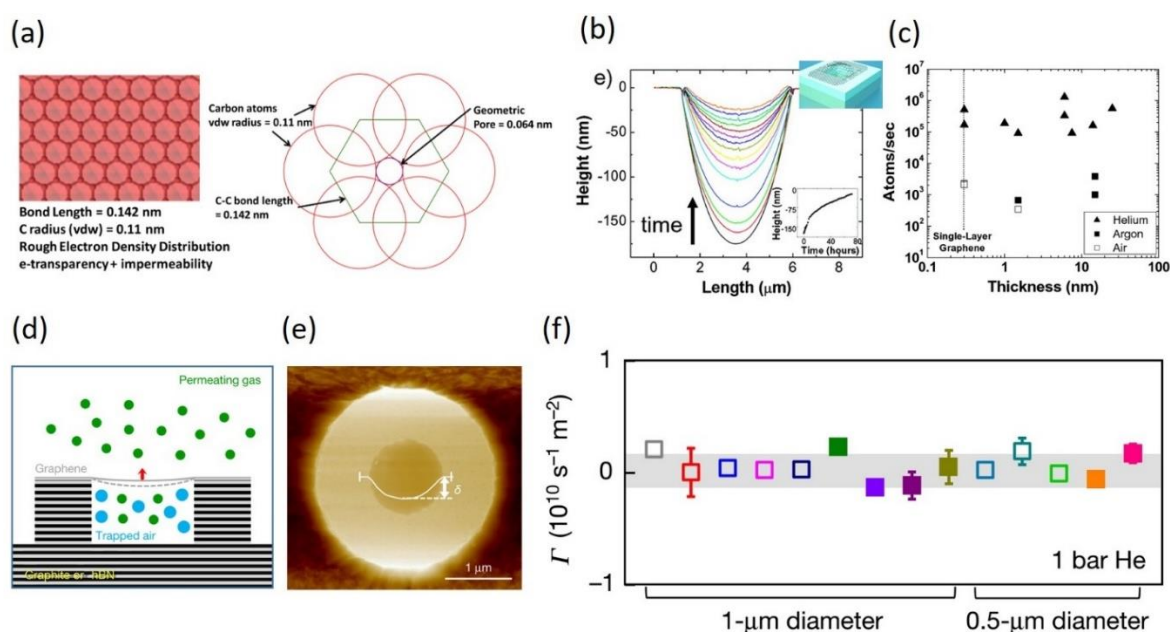
153 Note: AA: Aluminium alloy; ABA: 4-aminobenzoyl acid group; APTES: 3-(Aminopropyl) triethoxysilane; BA: Boric acid; CB: Carbon black; CR: cold-rolled;
154 CS: Carbon steel; CVD: Chemical vapor deposition; EIS: Electrochemical impedance spectroscopy; EVOH: Poly(vinyl alcohol-co-ethylene); GO: Graphene
155 oxide; ICR: Interfacial contact resistance; IL: Ionic liquid; MS: Mild steel; PPA: Polyphosphoric acid; PVA: Polyvinyl alcohol; PVB: polyvinyl butyral; SS:
156 Stainless steel; SST: Salt spray test; WPU: Waterborne polymer.

157

158 2.1. Graphene-based monolithic coating

159 2.1.1. Corrosion protection mechanism

160 Albeit being only one-atom thick, pure defect-free graphene can be completely impermeable to gases
161 (neon, nitrogen, oxygen, argon, krypton and xenon) and liquids, thus inducing the barrier effect to
162 protect the coated metal or steel surface from corrosion reactions [58]. This impermeability is mainly
163 due to the hexagonal lattice structure of graphene, where a geometric pore size of diameter 0.064 nm is
164 formed (Fig. 2a), which is even smaller than the helium atom [58]. The impermeability has been
165 demonstrated through a graphene-sealed microchamber. The deflation in air was captured by slowly
166 decreasing bubble deflection, as shown in Fig. 2b. The leak rate was estimated by monitoring the
167 pressure change which reached 10^5 – 10^6 atoms/s for helium (Fig. 2c) [59]. More recently, Sun *et al.*
168 fabricated a new type of microwells with impermeable monocrystalline walls (Fig. 2d and 2e), and
169 found the leakage rate to be as low as 10^{-4} atoms/s, enabling the permeation of just a few helium atoms
170 per hour (Fig. 2f) [60]. In addition, the high chemical stability of graphene further improves the
171 oxidation resistance of coatings and leads to passivation of the metal underneath in the active oxidation
172 environments [61].



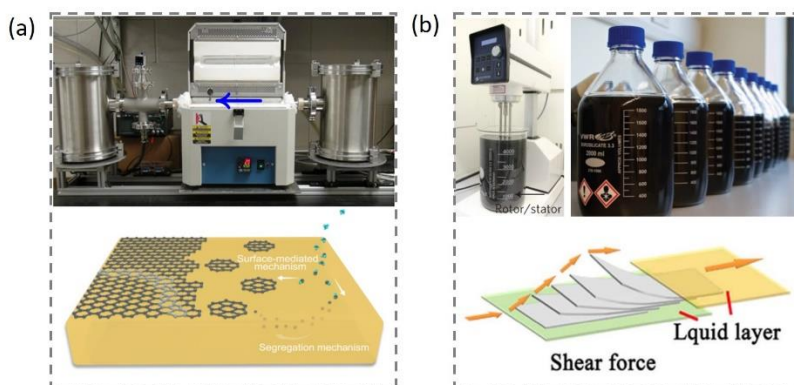
173

174 **Fig. 2** (a) Atomic structure of monolayer graphene with rough electronic density distribution. Reproduced with permission
175 from Ref. [58]. Copyright 2013, Elsevier. (b) The AFM line profile of inward bubble deflection showing the air leakage over
176 time. (c) Leakage rate as a function of graphene thickness for different gases. Reproduced with permission from Ref. [59].
177 Copyright 2015, American Chemical Society. (d) Schematic and (e) AFM image of graphene-sealed monocrystalline
178 microchamber. (f) Leakage rate evaluated based on 14 samples placed in helium over a one-month period. Reproduced with
179 permission from Ref. [60]. Copyright 2020, Springer Nature.

180 2.1.2. Preparation/coating methods

181 The most straightforward way to cover a metal substrate with a graphene-based monolithic (single or
182 few layer) coating is to simply synthesize graphene film directly on to its surface. Chemical vapour
183 deposition (CVD) is a commonly used method (Table 1) for the large-area synthesis of graphene films
184 (Fig. 3a). It not only allows a direct, facile, large-scale and transfer-free graphene coating process, but
185 also affords graphene production with good quality, coverage uniformity and a clean interface with the
186 underlying metal materials [62,63]. A direct growth of graphene on different types of steel can be
187 achieved using low-temperature methods [63].

188 Mass production of graphene for anti-corrosive coating can also be realized by liquid exfoliation. In
189 particular, graphene nanoplatelet (GNP) can be separated from graphite in aqueous solutions through
190 sonication, accompanied with an oxidation-reduction process [64]. The key issue here is the presence
191 of excessive structural defects within the graphene lattice. In contrast, liquid phase exfoliation has been
192 demonstrated to offer a scalable and cost-effective route to produce high-quality, unoxidized graphene
193 from powdered graphite [65]. The high-shear liquid exfoliation is able to achieve the exfoliation in
194 liquid volumes from hundreds of millilitres up to hundreds of litres and beyond (Fig. 3b) [66]. These
195 dispersions can then be used to deposit flakes by dip coating, spray coating and other coating methods.



196

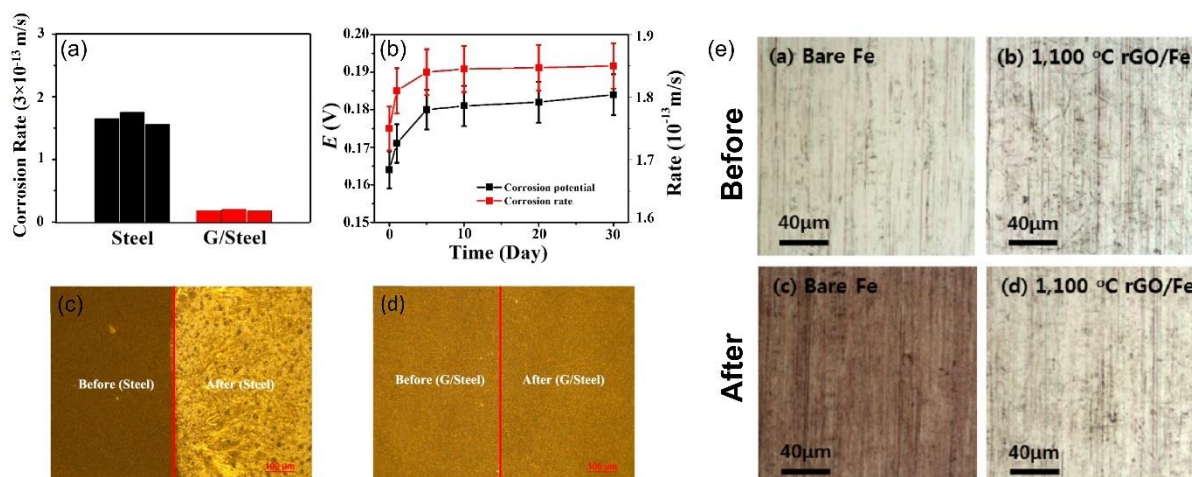
197 **Fig. 3** (a) Chemical vapour deposition system configured for graphene growth on metallic substrate. Reproduced with
198 permission from Ref. [62]. Copyright 2018, American Chemical Society. Reproduced with permission from Ref. [67].
199 Copyright 2015, Springer Nature. (b) Scalable production of few-layer graphene with high-shear liquid exfoliation method.
200 Reproduced with permission from Ref. [66]. Copyright 2014, Springer Nature. Reproduced with permission from Ref. [68].
201 Copyright 2014, The Royal Society of Chemistry.

202 2.1.3. Anti-corrosion performance

203 CVD grown graphene coating has been demonstrated to protect the surface of steel from corrosion as
204 evidenced in the literature summarized in Table 1. Facing the challenge to synthesize graphene directly
205 on steels, Zhu *et al.* proposed a generalizable low-temperature ($\sim 300^{\circ}\text{C}$) CVD method to fabricate large-
206 area and low-defect graphene-based monolithic coatings with single to few layers [39]. Electrochemical
207 corrosion results showed that the corrosion rate of graphene-coated stainless steel was reduced by 9
208 times compared to bare steel (i.e., non-coated steel) without graphene protection, as shown in Fig. 4.
209 Even immersed in a sea salt solution (5%) for 30 days, the corrosion rate maintained relatively low with
210 graphene coating, which indicated an effective anti-corrosion performance in harsh environment [39].
211 To facilitate the graphene growth on carbon steel, Ye *et al.* adopted a laser induction technique to
212 introduce nickel element into carbon steel and overcame the CVD temperature limitation [40].
213 Electrochemical impedance spectroscopy (EIS) was carried out following 1 h immersion of samples in
214 3.5% NaCl aqueous solution. The results indicated that the corrosion rate for graphene-coated carbon
215 steel was much less compared to that of bare stainless steel. The corrosion resistance could reach a high
216 level, almost 7 times that of bare carbon steel and comparable to that of bare stainless steel [40]. More
217 quantitative descriptions are detailed in Table 1.

218 While graphene oxide (GO) films fail to provide effective shielding against gases and liquids mainly
219 due to the loose stacking and defective structures [69], the chemical or thermal reduction aids to reduce
220 the interlayer separation and restores the graphene lattice by removing oxygen functional groups [70].
221 It is therefore, reasonable to expect an improvement in corrosion resistance for reduced GO (rGO)
222 coatings, since the properties of rGO is somewhat comparable to pristine graphene. Mayavan *et al.*
223 indicated that the rGO monolithic coating is more capacitive than resistive, hence, providing protection

224 against corrosion of iron [41]. Bagherzadeh *et al.* coated rGO nanosheets on carbon steel and realized
 225 a 67.2% increase in protective efficiency on rGO-coated carbon steel compared to their bare counterpart
 226 [42]. A reduction up to three times in the corrosion rate was observed, accompanied with an increase in
 227 charge transfer resistance and a decrease in corrosion current (Table 1) [43]. The high degree of
 228 oxidation resistance of the rGO film is exemplified in Fig. 4e, where the colour of the bare iron changed
 229 to brown after oxidation while the rGO-coated iron remained almost unchanged [71].



230
 231 **Fig. 4** (a) Corrosion rates of stainless steel and graphene/stainless steel (G/steel) samples. (b) Corrosion potentials and
 232 corrosion rate as a function of the time in the G/steel sample. Optical images of (c) pure stainless steel and (d) G/steel substrate
 233 before and after electrochemical anticorrosion testing. Reproduced with permission from Ref. [39]. Copyright 2016, American
 234 Chemical Society. (e) Optical images of bare and rGO-coated iron foils before and after oxidation at 200 °C in air for 2 h.
 235 Reproduced with permission from Ref. [71]. Copyright 2012, American Chemical Society.

236
 237 Durability performance of steel rebar within concrete is a vital factor in civil infrastructure. Corrosion
 238 performance of a carbon steel rebar coated with GO (drop casting several times along with electron
 239 reduction) was investigated in a simulated concrete pore solution with 3 wt.% NaCl [44]. This was to
 240 provide an understanding of the durability performance of GO coated steel rebar embedded in a concrete
 241 matrix. GO coating reduced the corrosion current by almost three times to that of uncoated steel rebar.
 242 This resulted in a nearly 95 times reduction in corrosion rates of GO coated steel rebar (0.85 mm/yr)
 243 compared to uncoated steel rebar (0.85 mm/yr).

244 2.2. Graphene-based laminate coating

245 2.2.1. Corrosion protection mechanism

246 Graphene-based laminate coating, featuring multi-layered heterogeneous structures with alternating
 247 materials (e.g. polymer, ceramic, etc.), is proposed to build a thicker barrier on the metal surface.
 248 Typically, ceramics or polymers are deposited on graphene-based monolithic coatings as protective
 249 layers. For example, the alumina films with only a few atoms in thickness have exhibited outstanding
 250 impermeability to standard gases (e.g. oxygen), thanks to their pinhole-free structures [72]. These
 251 protective layers can not only passivate the defects in graphene but also minimize the external effects,
 252 such as mechanical scratches or local heating. Coatings can be subjected to complex stresses during
 253 practical use scenarios. Depositing several thin layers which have different mechanical properties can
 254 help to reduce the stress concentration and change crack propagation conditions [73]. The multi-layered

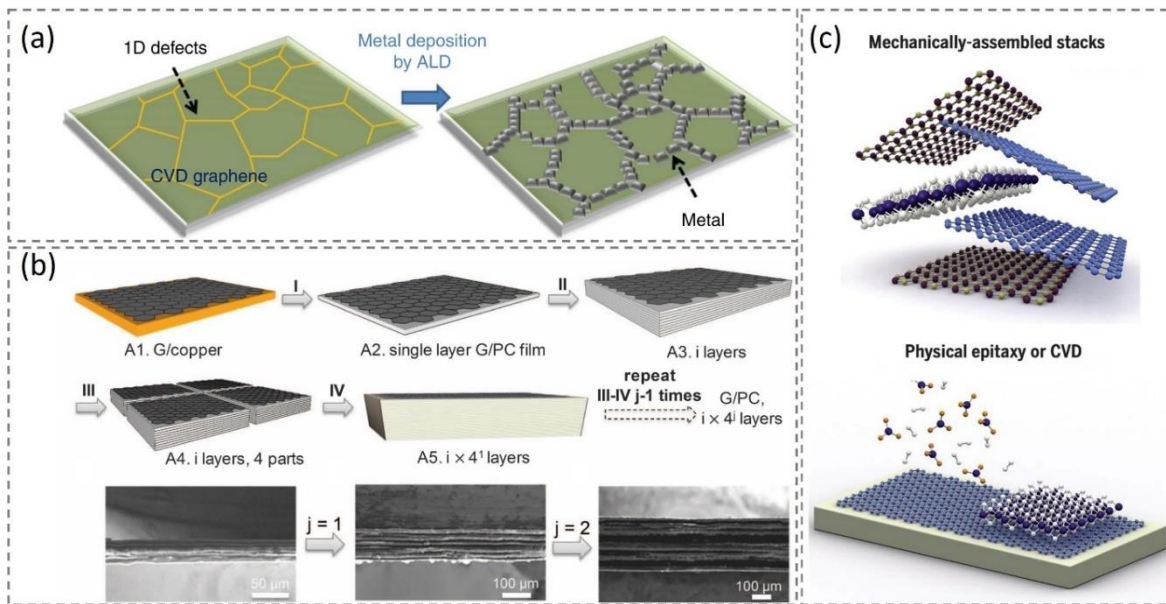
255 structure can be more compact and ordered for graphene coating composed of nanoplatelets, with the
256 potential to markedly suppress cohesive failure. In addition to the structural protection and the
257 passivation of defects, the introduced protective layers are insulating and therefore, also serve to break
258 the galvanic coupling between graphene and metal substrate. In this respect, the insulating nature of
259 hexagonal boron nitride (hBN) can reduce galvanic corrosion [74]. Moreover, hBN has the same
260 hexagonal structure as graphene and therefore also possesses similar impermeability and mechanical
261 strength [75,76], which makes the vertically stacked graphene/hBN heterostructure coating more
262 promising in corrosion prevention applications than pure graphene-based monolithic coating, especially
263 for the requirement of nanoscale thickness for anti-corrosive coatings.

264 **2.2.2. Preparation/coating methods**

265 Among thin film fabrication techniques, atomic layer deposition (ALD) has demonstrated potential
266 advantages in producing dense and uniform ultrathin films/coatings [77–79]. The ALD process involves
267 self-limiting surface reactions from the gas phase with atomic monolayer precision. This permits perfect
268 conformal coatings for thin films, even on surfaces with complex shapes [80]. More importantly, as the
269 C–C bonds in heptagon-pentagons present in the grain boundaries in graphene are highly strained and
270 reactive, the ALD allows the selective deposition of metal or metal oxide on graphene’s grain
271 boundaries and cracks due to the enhanced chemical reactivity (Fig. 5a) [81,82]. By controlling the
272 deposition parameter, ALD layer thickness can be increased to achieve the complete sealing of surfaces,
273 which would benefit the anti-corrosion performance of the laminate coatings.

274 The laminate coating can also be fabricated through an alternative stacking of graphene and polymer
275 layers (Fig. 5b). In particular, layer-by-layer assembly is well acknowledged as an efficient route for
276 manufacturing highly ordered multilayer film structures. The advantages of this technique include the
277 versatility of substrate options, the nanoscale control over the film thickness, the precise tailoring of
278 graphene-polymer interface and the fine tuning of the surface morphology [83,84]. By far several
279 deposition methods have been demonstrated for the layer-by-layer processing, such as dip coating, spin
280 coating, spray coating, vacuum filtration, Langmuir-Blodgett deposition and so forth [85].

281 Regarding the graphene/hBN hybrid coating, in situ CVD growth method with practical scalability,
282 high uniformity and quality has been documented [86]. However, the most versatile technique for the
283 construction of heterostructure is direct mechanical assembly (Fig. 5c) [87]. Recently, state-of-the-art
284 transfer methodologies have been comprehensively reviewed, such as polydimethylsiloxane (PDMS)
285 exfoliation, vdW pick-up and PMMA (polymethyl methacrylate) carrying layer method [88,89].

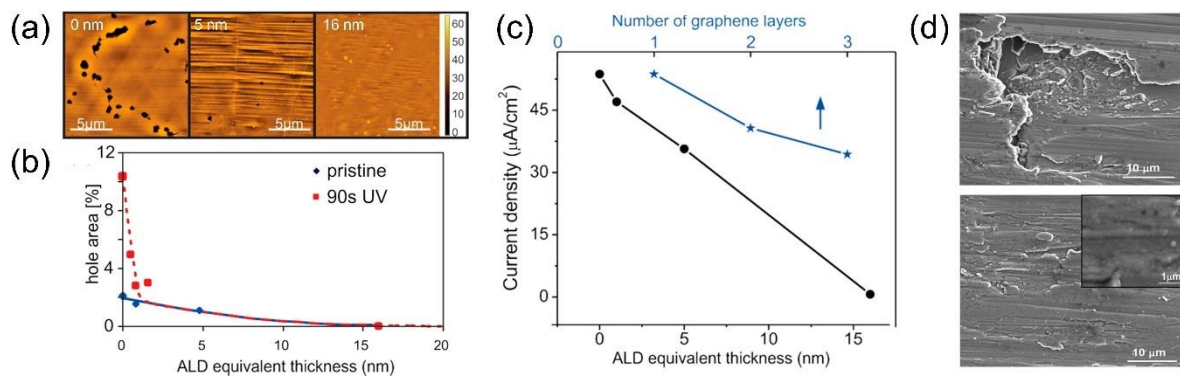


286

287 **Fig. 5** (a) Selective platinum growth by ALD on one-dimensional defect sites of polycrystalline CVD graphene. Reproduced
 288 with permission from Ref. [81]. Copyright 2014, Springer Nature. (b) Fabrication of graphene/polycarbonate layers with
 289 aligned CVD, comprising spin coating, etching and stacking procedures. Reproduced with permission from Ref. [90].
 290 Copyright 2016, The American Association for the Advancement of Science. (c) Production of van der Waals heterostructures,
 291 including mechanically assembled stacks and large-scale growth by CVD or physical epitaxy. Reproduced with permission
 292 from Ref. [87]. Copyright 2016, The American Association for the Advancement of Science.

293 2.2.3. Anti-corrosion performance

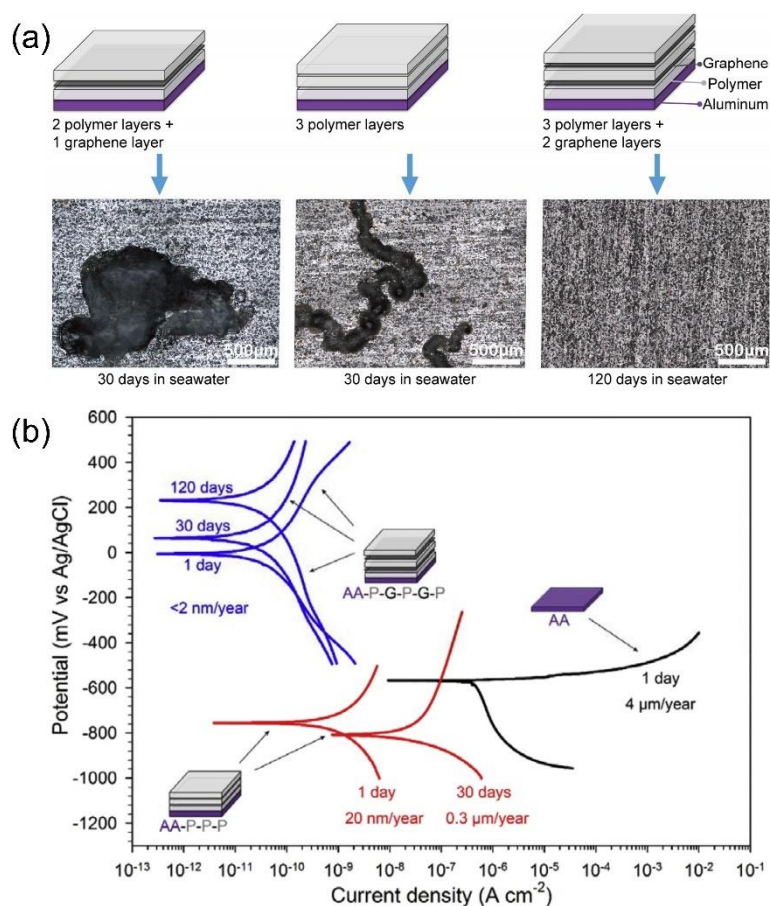
294 Improved anti-corrosion performance has been reported for CVD grown graphene coating covered with
 295 ALD alumina layer (Table 1). By tuning the size of ALD-generated particles and ALD cycles, the
 296 openings in the graphene coating could be selectively passivated, as evidenced by AFM images showing
 297 the change in morphology (Fig. 6a). As the ALD film thickness increases, a decrease in etch pit density
 298 can be observed. The continuous film is formed after 160 ALD cycles (Fig. 6b), which correspondingly
 299 leads to an inhibition efficiency of >99% (Fig. 6c) [47]. Mondal *et al.* further deposited alternating
 300 layers of alumina (Al_2O_3) and titanium dioxide (TiO_2) on rGO films by ALD technique and studied the
 301 anti-corrosion performance of such laminate coatings on stainless steels [45]. While the individual layer
 302 coating (rGO or $\text{Al}_2\text{O}_3/\text{TiO}_2$) failed to provide the corrosion protection alone, the combined laminate
 303 coating proved to be stable and resistive against pitting (Fig. 6d). The increased impedance of the
 304 interface and the pitting potential (Table 1) could be attributed to barrier effect of the film and shielding
 305 of the local electrical fields [45].



306

307 **Fig. 6** (a) AFM topography image of etched graphene with ALD film of different thicknesses. (b) Copper hole area after
 308 deposition of ALD films on graphene coating. (c) corrosion current density as a function of ALD film thickness. Reproduced
 309 with permission from Ref. [47]. Copyright 2014, American Chemical Society. (d) SEM images of Al₂O₃/TiO₂ coating with
 310 and without rGO on stainless steel after 30 days of immersion in neutral pH, 3.5 mass% NaCl aqueous solution. Reproduced
 311 with permission from Ref. [45]. Copyright 2016, Elsevier.

312 Polymeric materials have also been widely used in layer-by-layer assembly with graphene for the anti-
 313 corrosion applications. Yu *et al.* prepared a series of CVD graphene/polymer laminate coatings through
 314 a spin coating-assisted assembly process (Fig. 7a) [91]. By conducting electrochemical tests, it was
 315 found that the pure polymer coating failed in protecting the metal after less than 30 days, while the
 316 laminate coating exhibited a higher corrosion resistance (Fig. 7b and Table 1). The corrosion protection
 317 mechanism rests on the construction of the laminate structure, which exploits the impermeability of
 318 graphene as well as the adhesive and insulating properties of the polymer layers [91]. Researchers have
 319 also reported the corrosion prevention applications of hBN films in marine coatings applied on stainless
 320 steel [48]. Recently, the effect of stacked MoS₂/hBN vdW heterostructure coating on the corrosion
 321 behaviour of steel (SS304) has been investigated. By comparison, the incorporation of hBN in between
 322 MoS₂ layers was found to improve its corrosion resistance as hBN layers constrained the charge carrier
 323 mobility [92]. Thus, it can be envisioned that graphene coating would also benefit from having hBN
 324 layers intercalated so that the galvanic coupling could be blocked to prolong the lifetime of coating.



325 **Fig. 7** (a) Corrosion morphology and (b) Potentiodynamic scans for bare polymer and polymer/graphene laminate coatings
 326 after long-lasting immersion in 3.5 wt% NaCl solution. Reproduced with permission from Ref. [91]. Copyright 2018, Elsevier.
 327

328

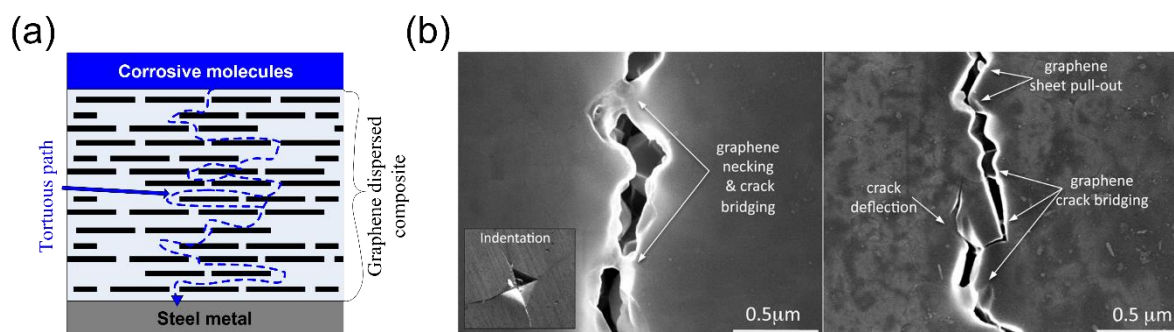
329

330 2.3. Graphene-based nanocomposite coating

331 2.3.1. Corrosion protection mechanism

332 Adding graphene and its derivatives as fillers into conventional organic coatings represents another
333 protection strategy pertaining to the corrosion of metals. This approach mainly takes advantage of the
334 chemical inertness and corrosion resistance of graphene to extend the propagation path length of the
335 corrosion medium in the coatings. As shown in Fig. 8a, the diffusion pathway of corrosive molecules
336 such as H₂O, Cl⁻ is considerably twisted and prolonged by the graphene materials is termed as tortuous
337 path effect. Such a barrier mechanism endows polymer/graphene nanocomposite with a higher potential
338 in advanced anti-corrosive coating material compared with traditional polymer/clay composites [54].

339 Additionally, graphene aids to effectively prevent or retard cracking by strengthening and toughening
340 the polymer film coating. This is possible by way of the following mechanisms: (i) graphene fillers can
341 efficiently bear the load through the stress transfer across interfaces so as to improve the fracture
342 resistance of the coating [93–95]; and (ii) once cracks are initiated and propagated into polymer matrix,
343 they can be deflected/blunted by graphene to increase the crack pathway required to fracture the material
344 [96,97]. Meanwhile, the weak interactions between graphene and the polymer matrix facilitate the
345 interfacial sliding and result in graphene pull-out and crack bridging (Fig. 8b) [98,99]. These
346 phenomena all induce more energy dissipation and account for the toughening mechanism. The
347 consequent delay of crack propagation increases the duration and service life of graphene
348 nanocomposite coatings.



349
350 **Fig. 8** (a) Schematic of tortuous path effect. (b) Typical fracture toughening mechanisms in graphene-based nanocomposite.
351 Reproduced with permission from Ref. [96]. Copyright 2011, American Chemical Society.

352

353 2.3.2. Preparation/coating methods

354 The graphene-based nanocomposite coatings are commonly prepared with polymer-based GNP or GO
355 dispersed compounds. Depending on the graphene filler types, different techniques and coating
356 processes have been adopted for improved coating and anti-corrosion performance (Table 1). Typically,
357 GNP/polymer-based nanocomposite coatings are produced through dispersing GNP in epoxy with
358 solvents and acids using either or combination of magnetic stirring, roll mill and ultrasonication
359 techniques at different temperature and mixing sequencing, then casting of GNP-polymer solution on
360 steel substrates. GO/polymer-based nanocomposite coatings, on the other hand, are produced either by
361 direct mixing of GO in polymer, or most popularly water/solvent borne GO in polymer-based
362 composite; subsequently, drop casting, bar coater and spray gun can be used for coating over steel
363 substrate. However, it should be noted that, direct mixing of GO without the aid of any solvent or water
364 is found not to be a promising approach for coating steel metal surface. The is due to the fact that

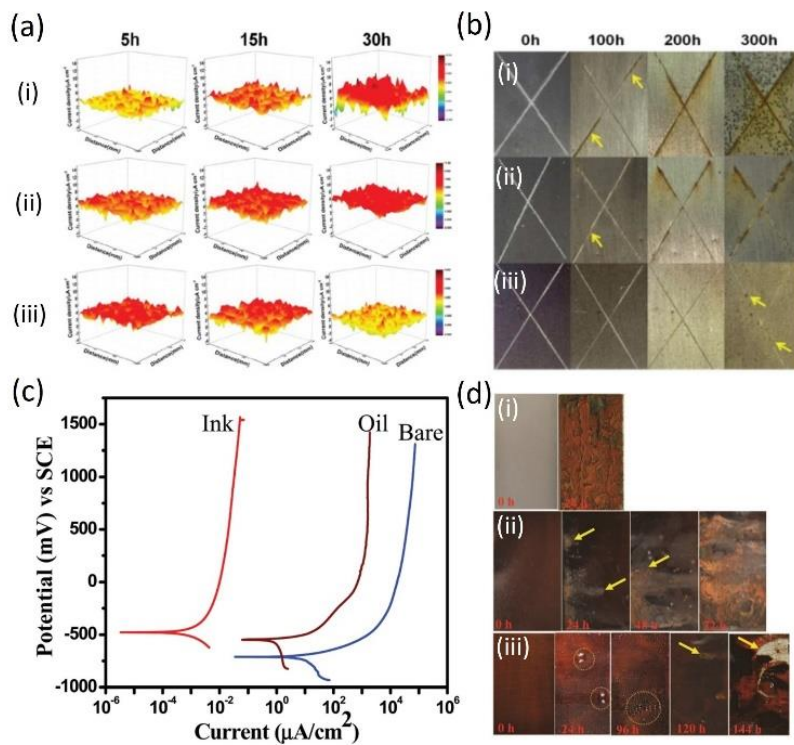
365 effective dispersion of GO nanofillers in the polymer base media is the key issue to produce desirable
366 polymer nanocomposite coating, and wet transfer method with rigorous mixing is typically used to
367 achieve this desirable state. The surface functionalization of GO is crucial to the interface design and
368 performance control of GO/polymer nanocomposite coating [100]. Typically, amino polymers, silanes,
369 amines, ionic liquids and nanoparticles are used for the functionalization of GO, which encourage
370 reactions between amine and epoxy, amine and carboxyl or salinisation for improved coating
371 performance [101]. The functionalization of GO improves the interaction between GO and epoxy resins,
372 as well as reduces the aggregation potential of GO sheets. In addition, the solvents used for preparation
373 of solvent borne epoxy/GO nanocomposite coating are typically low-polar solvents used in painting
374 applications [101]. Experiments have shown that GO is hydrophilic in nature [102]. When studying the
375 effect of organic solvents, different interactions become relevant, for example, dispersion interactions,
376 donor-acceptor, and electrostatic interactions in the presence of ions. Furthermore, the desired outcome
377 also depends on the polarity of the solvent used [103].

378 **2.3.3. Anti-corrosion performance**

379 Effective composition of 2D graphene with the base materials eliminates the limitations of coating
380 bonding with steel substrate and impacts of graphene defects on the corrosion mechanisms, thus
381 yielding superior anti-corrosion performance on steel compared to that of graphene-based monolithic
382 coating and laminate coating, as indicated in Table 1. For instance, roller coating and subsequent
383 imidization of the nanocomposite blends yielded well-adhered GNP/polyetherimide (PEI) coating on
384 steels. Potentiodynamic testing and sea salt water immersion tests indicated more than three orders of
385 enhancement in efficacy of corrosion protection as compared with bare low-alloy steel. The inclusion
386 of graphene also reduces corrosion by an order of magnitude over the pure polymeric coating [104].
387 Upon application of highly crystalline graphene integrated polyaniline nanostructured composites as
388 corrosion protection coatings, Mahato *et al.* reported a decline in corrosion current up to ~3–4 orders
389 of magnitude for coated mild steel surface in 0.1 M HCl [105]. Similar anti-corrosion performance was
390 also observed for a hydrophobic epoxy/graphene nanocomposite coating on cold-rolled steel surface as
391 detailed in Table 1 [55].

392 GO/polymer-based nanocomposite coating shows considerable efficiency in the anti-corrosion
393 performance as well. Liu *et al.* studied the anti-corrosion performance of imidazole ion grafted GO
394 composite [51]. The salt spray test results indicate that pure epoxy and rGO/epoxy coated steel
395 substrates corrode at the scratch after immersing in NaCl solution for 100 h, while imidazole ion grafted
396 GO/epoxy-based hybrid composite coating protects the steel surface from corrosion even after 300 h
397 (Fig. 9b). Furthermore, the hybrid composite coated steel shows the minimal corrosion current and
398 highest interfacial adhesion compared with other two systems (Fig. 9a). These observations indicated
399 that the imidazole ion grafted GO/epoxy hybrid coating effectively enhanced the anti-corrosion
400 performance of steel as well as prevented the detachment of coating from the steel surface. Singhababu
401 *et al.* studied an oil-based GO ink for anti-corrosive coating of cold-rolled steel [52]. The evaluation of
402 the corrosion properties in the cold-rolled steel substrates from the open circuit potential measurements
403 shows that the potential moves towards the positive potential by the coating of oil and a greater shift is
404 observed in GO ink-coated steel substrate (Fig. 9c). The corrosion rate of bare cold-rolled steel is found
405 to decrease by over 10,000 times with assistance of the GO-ink coating (Table 1). Another study
406 similarly reported that a rGO sunflower-based ink coating suppressed the corrosion rate of cold-rolled
407 steel by nearly 10,000 times compared to bare cold-rolled steel [53]. The red rusting in the cold-rolled
408 steel due to the salt spray test initiated in GO-ink coated cold-rolled steel after 100 h in contrast to that
409 of 24 h and 6 h for the oil-coated and bare steel, respectively (Fig. 9d). Overall, the oxygen functional
410 groups of oil may result a chemical bonding with the metal and GO which produce an impermeable

411 coating layer with good adhesion on the steel surface. In fact, these values are higher than the reported
 412 corrosion rate of composite coatings containing polyaniline/graphene (10 times) [54], epoxy/graphene
 413 (4 times) [55], ceramic/graphene (150 times) [45], silane/functionalized GO (130 times) [106], and
 414 PMMA/rGO (7 times) [107]. The corrosion protection and durability performance of steel rebar coated
 415 (with GO, rGO, and MWCNT mixed to two-part epoxy resin) embedded in concrete was investigated
 416 [57]. The average mass loss following accelerated corrosion testing of uncoated steel rebar in concrete
 417 saturated with NaCl was 24.5%. In comparison, the mass loss decreases for PE, rGO/CNT, GO/CNT
 418 coated rebar to 11.3%, 8.6%, 0.45%, respectively relative to the uncoated steel rebar [57]. These results
 419 indicate a direct improvement in corrosion resistance of rGO/CNT coated rebars by 65% and 24%,
 420 respectively, compared to uncoated and PE coated rebars. However, the greatest durability performance
 421 was observed in the GO/CNT coated rebar where minimal corrosion was observed even after 150 days.
 422 More details are provided in Table 1.



423

424 **Fig. 9** (a) Scanning vibrating electrode technique maps of current density and (b) digital images of salt spray-test for (i) pure
 425 epoxy, (ii) rGO/epoxy and (iii) imidazole ion grafted GO/epoxy coatings immersed in a 3.5 wt% NaCl solution. Reproduced
 426 with permission from Ref. [51]. Copyright 2018, The Royal Society of Chemistry. (c) Polarization behaviour in 3.5% NaCl
 427 aqueous solution and (d) digital images of salt spray test of (i) bare, (ii) oil coated, and (iii) GO ink coated cold-rolled steel.
 428 Reproduced with permission from Ref. [52]. Copyright 2015, The Royal Society of Chemistry.

429

430 3. Challenges and potential for graphene-based anti-corrosive coating with application to 431 structural steel and rebar for infrastructure application

432 The inspiring possibilities of graphene-based coating have encouraged major steel producers such as
 433 POSCO and Tata Steel to produce anti-corrosive graphene-coated steel [52]. However, industrial
 434 manufacturing of graphene-based coating is complicated by misaligned manufacture capability in
 435 laboratory and industry in terms of scale, cost, and quality, due to disparate goals, workflows, and
 436 standards. Furthermore, the durability and reliability of anti-corrosive coating over long-term usage is

437 of particular significance for industrial application. In the following subsections, the challenges and
438 potentials of graphene-based anti-corrosive coating on steel progressing in future will be discussed from
439 the perspectives of long-term stability of coatings as well as scalability, cost-effectiveness, quality and
440 environmental sustainability of industrial processing. The discussion is based on the detailed assessment
441 of existing studies on graphene-based coating as summarized in Table 1.

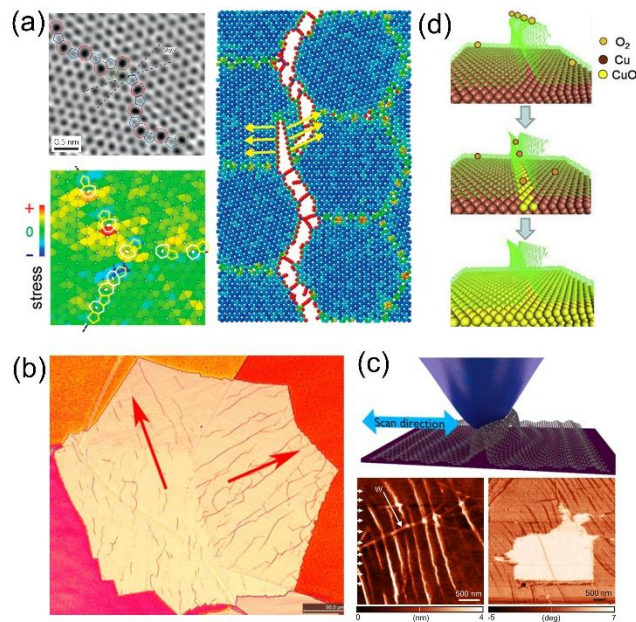
442 **3.1. Long-term stability**

443 The long-term stability is one of the key practical requirements for graphene-based anti-corrosive
444 coating. Specifically, both the mechanical durability (resistance to cracks, wear, fatigue) and
445 environmental durability (stability against humidity, temperature, chemicals) principally rely on the
446 structural integrity and interfacial adherence of the coating.

447 (1) *Graphene-based monolithic coating*: The defective nature of commercially available graphene
448 and its relative weak adhesion to the rough steel structures limit the long-term anti-corrosion
449 performance for graphene-based monolithic coating. In particular, as shown in Fig. 10a, tilt
450 boundaries usually form during the CVD growth due to the accumulation of dislocations and
451 are considered as linear defects [108]. These defects, on one hand, act as reactive sites to
452 facilitate the localized corrosion of steel in exposed areas. On the other hand, they easily induce
453 the stress concentration and serve as the nucleation centres for cracks (Fig. 10a) [109,110].
454 Therefore, it is conceivable that grain boundaries render the CVD graphene-based coatings
455 vulnerable to fracture and can lead to catastrophic failure due to the brittleness of graphene
456 [111]. Likewise, other intrinsic defects such as atomic vacancies were found to accelerate the
457 local corrosion owing to an incomplete coverage and consequent galvanic coupling between
458 graphene and metal [112,113]. Such defect-related problems are also inevitable in graphene
459 coatings consisting of micro-sized GNP or GO derived from sonication or liquid exfoliation. In
460 this regard, in-plane defects of graphene can be compensated by vertically stacking multiple
461 graphene layers, which prolongs corrosion pathway and increase the oxidation energy barrier
462 to block the diffusion [114–116].

463 Apart from the structural integrity, CVD-grown graphene suffers from prominent surface
464 corrugations, as a result of macroscopic roughness of metal substrate and the strain relief
465 attributed to the thermal expansion (Fig. 10b) [117]. Solution-based graphene also easily
466 wrinkles during the processing and deposition [118]. This would lead to interface defects (e.g.
467 buckles) that impair the conformal contact and weaken the adhesion between graphene and the
468 substrate, resulting in the tear and peeling failure of the coating (Fig. 10c) [119,120]. Moreover,
469 buckles can be deemed as micro-channels to allow the intercalation and lateral diffusion of
470 oxygen atoms (Fig. 10d). Considerable strains within buckles further aid to enhance the
471 chemical reactivity and enable an easier etching of graphene, which is detrimental to the long-
472 term anti-corrosion performance [117,121]. Then again, such interfacial issues can be further
473 magnified for structural steels and rebars with highly rough and nonplanar surfaces.

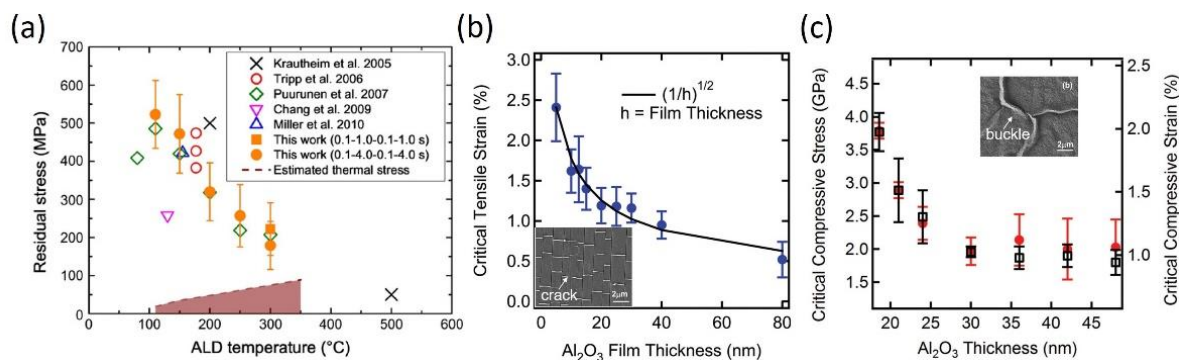
474
475 The long-term durability of the coating on the steel is another practical and mechanistic
476 consideration which is affected by its surrounding environment. Steel rebar in concrete, for
477 example, undergoes extensive mechanical loading [122], friction, shrinkage [123], fatigue
478 [124], extreme weather [125], and potentially harsh chemical exposure (chloride, carbonation,
479 sulphate attack) [126,127] exposure for several decades. Long term corrosion, scratch and
480 abrasion resistance of high precision monolithic coating could be compromised in case of
481 extremely thin and sensitive coating and therefore warrants investigation.



482

483 **Fig. 10** (a) Grain boundaries in CVD grown polycrystalline graphene with non-uniform stress distributions. Reproduced with
 484 permission from Ref. [108]. Copyright 2014, Springer Nature. Reproduced with permission from Ref. [109]. Copyright 2013,
 485 American Chemical Society. (b) Optical image of CVD grown graphene after annealing in air, showing distributed wrinkles.
 486 Arrows indicate the oxidation lines along the wrinkles. Reproduced with permission from Ref. [117]. Copyright 2014, AIP
 487 Publishing. (c) AFM probe scanning induced peeling-off of graphene from the substrate. Reproduced with permission from
 488 Ref. [119]. Copyright 2016, Elsevier. Reproduced with permission from Ref. [120]. Copyright 2017, American Chemical
 489 Society. (d) Corrosion process of graphene with wrinkles on metal substrate. Reproduced with permission from Ref. [121].
 490 Copyright 2014, Elsevier.

491 (2) *Graphene-based laminate coating*: As known, thin films and functional coatings can develop
 492 significant residual stresses as a pervasive consequence of solid materials processing (Fig. 11a),
 493 which is always a major concern in technological applications from a reliability and
 494 performance point-of-view [128]. Worst case scenarios might manifest as an isolated crack,
 495 connected channelling or an adhesion failure, depending on the material composition and
 496 property, stress states and local flaws [129]. Specifically, under the tensile stress, a brittle
 497 coating (e.g. atomic layer deposited ceramic coating) may fracture by the growth of cracks
 498 through the thickness of the film, while a relatively tougher coating (e.g. spin-cast polymer
 499 coating) may fail by delamination along the interface (Fig. 11b). Instead, the failure mechanism
 500 associated with a compressive stress in the coating usually involves simultaneous buckling and
 501 delamination (Fig. 11c) [130]. Both the cracks and delamination create diffusion paths allowing
 502 corrosive species to pass through the thickness or via the coating/metal interface to diminish
 503 the barrier function. On the other hand, in service, stresses may arise slowly and cause failure
 504 to occur at much lower values compared to theoretical strength. Such a fatigue failure either in
 505 crack or adhesive mode may become more severe in the coating with nonuniform stresses,
 506 especially for the layer-by-layer assembled laminate coating [98,131]. However, the effective
 507 sealing by conformal ceramic or polymer coating offers additional protection for structural steel
 508 and rebars. In addition to defect patching, the adhesion to the substrate can also be improved
 509 by for example introducing an adhesive polymer layer, which allows application of laminate
 510 coating to curved and rough surfaces. Hence, the graphene-based laminate coating is reasonably
 511 considered to provide the medium-term corrosion protection for structural steels and rebars.



512

513 **Fig. 11** (a) Summary of residual stress of ALD Al₂O₃ film as function of ALD temperature. Reproduced with permission from
 514 Ref. [132]. Copyright 2014, Elsevier. Critical (b) tensile and (c) compressive strains for cracking of Al₂O₃ films as a function
 515 of film thickness. The insets are SEM images of cracks under tensile stress and buckles under compressive stress. Reproduced
 516 with permission from Ref. [133]. Copyright 2011, AIP Publishing.

517 (3) *Graphene-based nanocomposite coating*: The primary factor in improving the corrosion
 518 resistance in polymer nanocomposites is the tortuosity. Hence, the dispersion and orientation
 519 of graphene fillers determines the penetration distance to reach the underlying substrate.
 520 However, high surface energy often leads to a high degree of agglomeration of dispersed
 521 graphene-based fillers at high content, which tends to impair the tortuous path effect. It has
 522 been reported that aggregation of graphene at a high dosage leads to an increasing water
 523 permeability through a nanocomposite coating [56,134]. In addition, consequent aggregates
 524 show inferior mechanical properties due to the comparatively weak interlayer interactions
 525 [135][136]. Hence, GO, rGO and other functionalized graphene are more commonly used for
 526 preparation of nanocomposite coating due to the enhanced dispersion and interfacial bonding
 527 performance. For example, polydopamine (PDA) has been widely used as a surface modifier
 528 due to its abundant catechol and amine groups that may strengthen the interfacial adhesion
 529 [137]. It was found that a thin layer of PDA coating could enhance the dispersibility of the
 530 PDA-coated GO sheets in organic solvents, providing reinforced barrier property for
 531 anticorrosion of graphene-based nanocomposite coating [138]. Furthermore, as an organic
 532 polymer, the insulating PDA can bind graphene with metal substrate as glue and inhibit
 533 galvanic corrosion simultaneously [139]. The existence of benzene rings in PDA that shares
 534 similarities with graphene structure also makes PDA a potential candidate media to heal
 535 graphene structure defects [140]. Inspired by mussel and nacre, Zhu et al. designed a bionic
 536 epoxy-(graphene-dopamine)-epoxy sandwich composite coating via electrodeposition. They
 537 noted that the hydrogen bonding between GO and dopamine, as well as the electrostatic
 538 interaction between $-\text{COO}-$ in GO and $-\text{NH}_3^+$ in dopamine assist the self-alignment of
 539 graphene parallel to the substrate when subjected to external electric field [141,142]. These
 540 highly parallel nanosheets tremendously increase the barrier effect of the coating and prolong
 541 the penetration path of the corrosive medium [143]. Generally, the incorporation of graphene
 542 into the conventional polymers not only takes advantage of the barrier effect of graphene for
 543 protection, but also improves the damage tolerance of the coating. The chemical and thermal
 544 stability combined with enhanced mechanical properties further contribute to the mechanical
 545 and environmental durability of the nanocomposite coating. The addition of graphene-based
 546 nanocomposite coating on steel provides complete coverage of surface by the adherent layer
 547 with strong interactions, which plays a vital role in long-term sustainability of the coating [50].

548

549

550 3.2. Scalability

551 While in-lab fabrication is normally benchtop-scale with low throughput, industrial manufacturing is
552 required to be scaled up, in terms of both the material production and coating process.

553 (1) *Graphene-based monolithic coating*: Although CVD method has been shown as a relatively
554 scalable process via roll-to-roll operations, it can produce graphene with lateral dimensions in
555 meter size, only on copper [144]. Further production up-scaling is fundamentally limited by the
556 efficiency in the phase change of carbon, as well as the complexity of steel materials required
557 in infrastructures. The steel has a very low catalytic activity for graphene growth and further
558 hinders the large-scale production required for civil infrastructure. In contrast, liquid-phase
559 exfoliation appears more promising in industrial-scale production of graphene. Particularly,
560 high-shear mixing of graphite was demonstrated to give graphene that is many times more
561 efficient than sonication which can be scaled-up to an industrial level [66]. The exfoliation can
562 be achieved in liquid volumes from hundreds of millilitres up to hundreds of litres and beyond.
563 In fact, many companies involved in the carbon business have already established programs on
564 graphene and GO production, and claimed production capabilities of thousands of tonnes/year
565 [145]. In this context, ready access to a coating process that enables the solution-based
566 deposition of graphene layers is required to realize “laboratory to industry” translation. Popular
567 methods used for coatings involve dip coating, spin coating, spray coating, sol-gel approach,
568 in-situ polymerization, and electrophoretic deposition [31]. Among these coating methods,
569 spray coating has proven effective at the industrial scale in terms of size, processing speed and
570 imparted durability, and is not limited to planar substrates [146,147].

571 (2) *Graphene-based laminate coating*: The assembly techniques for constructing laminate
572 materials, no matter for ALD or layer-by-layer, are mostly limited to small-scale proof-of-
573 concept demonstrations [148]. In principle, ALD is based on the exposure of a surface to a
574 precursor vapour and, therefore, many substrates can be coated simultaneously to increase the
575 scalability. However, such a scalability of ALD technique is more applicable to the
576 semiconductor industry, with limited working area. Furthermore, most abovementioned coating
577 methods lack the industrial scalability except for dip coating and spray coating, yet dip coating
578 is generally time-consuming and labor-intensive. This hinders the industrial implementation of
579 layer-by-layer assembly of graphene-based laminate coating via the combination of different
580 coating methods [149].

581 (3) *Graphene-based nanocomposite coating*: The preparation method and coating process of the
582 graphene composite anti-corrosive coating can be established based on the traditional coating
583 production process, which has detailed protocols and standard operating procedures in
584 production and shows good controllability and workability in industrial synthesis and
585 applications. In particular, the graphene-based nanocomposite coating methods such as epoxy
586 powder-based fusion-bonded electrostatic coating has been recognized as mature and accessible
587 industrially scalable methods.

588 3.3. Cost-effectiveness

589 A successful product design should deliver a balance between working performance and manufacturing
590 cost. Albeit often ignored in academic research, while cost reduction is the priority for industrial
591 development. Therefore, the cost-effectiveness associated with material production and coating process
592 is key to realistically adopting graphene-based coatings and embracing an ambitious industrial shift.

593 (1) *Graphene-based monolithic coating*: CVD growth method is effective to produce large-scale,
594 high-precision graphene coatings, yet the economic viability may be the principal challenge for
595 the industrial-scale manufacturing of high-quality graphene as the process cost is constrained
596 by the size of substrate, precursor type and energy cost. Comparatively, the use of cheap
597 feedstock and straightforward operation endows liquid-phase exfoliation with higher cost-
598 effectiveness. Additionally, spray coating offers rapid assembly times and is amenable to
599 automation, which is beneficial for cost reduction of graphene-based monolithic coating.
600 Despite the waste issue of dip coating as it typically requires more material than other
601 technologies, especially to submerge large substrates at industrial scales, solutions can be
602 reused for cost saving as long as cross-contamination remains low.

603 (2) *Graphene-based laminate coating*: Although ALD possesses a number of promising features,
604 it is still technically suffering from low material utilization efficiency and energy-intensive
605 nature [31]. The cost-effectiveness issue associated with the slow deposition rate is critical
606 especially for the industrial production, considering long cycle times and the layer-by-layer
607 nature of the deposition. Particularly, high aspect ratio substrates, such as steel rebars, may
608 require longer time to allow for the precursor gas to disperse into trenches and other three
609 dimensional features [150]. Taking advantage of natural forces (e.g. van der Waals interactions)
610 to form a multilayer, the layer-by-layer assembly requires less investment in manufacturing
611 infrastructure and energy compared with ALD technique. However, resource efficiency is also
612 a major issue for layer-by-layer assembly technologies in coating applications. As only very
613 thin 2D layers are deposited during each growth cycle, a significant amount of waste can be
614 expected [17].

615 (3) *Graphene-based nanocomposite coating*: Graphene-based nanocomposite coating excels in the
616 relatively lower production costs and sufficient availability. The solution processability of
617 graphene is an advantage for low-cost processing. On the other hand, out of various coating
618 methods, electrostatic coating, sol-gel approach, and in-situ polymerization for preparation of
619 nanocomposites are cost-effective coating methods. As reported, the unit cost of commercial
620 steel and alternative reinforcement rebar for corrosion protection are for steel bar (ASTM A615,
621 grade 60) 0.7 US\$/kg [151,152], galvanized coated bar 1.1 US\$/kg (converting 1.5 times to the
622 uncoated steel) [153], epoxy coated steel 1.2 US\$/kg [152,154], SS (ASTM A955-316L) 5.5
623 US\$/kg [152,154]. Graphene-based coating can be used as an effective coating of steel or to
624 upgrade galvanized and epoxy-based composite coating without much impact on production
625 cost but significant improvement in coating performance.

626

627 **3.4. Quality**

628 Industrial manufacturing also requires precise process control to assure the quality of graphene and
629 graphene-based coatings, which determines their corrosion protection performance and durability.

630 (1) *Graphene-based monolithic coating*: The synthesis of graphene has long been a bottleneck for
631 its wide application. While CVD graphene is recognized to have a high quality (i.e. uniform
632 thickness, large area, less defect), solution-based approach never produces 100% monolayer
633 graphene, but a statistical distribution of graphene stacks with lateral dimension limited to a
634 few micrometres [155]. One of the fundamental challenges of graphene production is run-to-
635 run variations in terms of graphene quality, involving defects, homogeneity, thickness and

636 doping. This is greatly dependent on the quality of the bulk starting materials sold by different
637 vendors. Another remaining challenge would be efficient quality assessment of the liquid
638 exfoliated nanosheets in industrial scale. The significant statistical variation in the quality of
639 graphene and lack of standards are somewhat detrimental to its commercialization [145].
640 Consequently, the obtained graphene-based monolithic coating is expected to exhibit an
641 inhomogeneous coverage on steel structures.

642 (2) *Graphene-based laminate coating*: ALD or layer-by-layer assembly techniques provide a more
643 reliable route to fabricate high-quality protective coatings. ALD is known to allow processing
644 dense and homogeneous thin films, by building one mono-atomic layer after another. Such an
645 atomic level control ensures that extremely thin films with high conformality to complex
646 structures can be processed. Furthermore, ALD is exceptionally effective at coating surfaces
647 that exhibit ultra-high aspect ratio topographies (e.g. steel rebar), providing a robust coating
648 with high-quality interfaces. Such advantages of precise control of thickness and composition
649 as well as nanoscale interface engineering can also be found in other solution-processing layer-
650 by-layer assembly techniques.

651 (3) *Graphene-based nanocomposite coating*: The quality of raw graphite and liquid-exfoliated
652 graphene and chemically synthesized functionalized graphene also influences the quality of
653 graphene-based nanocomposite. Parameters such as the flake size thickness (related to volume
654 concentration), functionalization, and dispersion state play a key role in the tortuous effect for
655 protection efficiency. Meanwhile, the dispersion issues have been deemed as roadblocks on the
656 journey of manufacturing of high-performance nanocomposites. While postprocessing may be
657 effective to alleviate these issues by additional procedures, the overall quality of nanocomposite
658 coating can be guaranteed by the standard manufacturing process using industrial-scale
659 equipment in a streamlined manner.

660 **3.5. Environmental sustainability**

661 Key issues such as environmental sustainability deserves special attention during the practical
662 applications. Many of the potential environmental impacts that can result from the industrial process
663 are related to chemical reactions that take place within a facility.

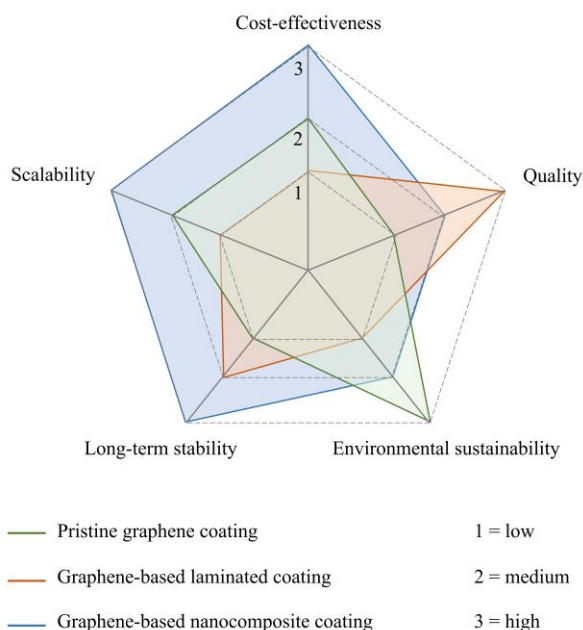
664 (1) *Graphene-based monolithic coating*: CVD method is suitable for high precision graphene
665 coating, yet there are hazard issues due to the use of toxic chemical precursors and generation
666 of reactions gas or liquid by-products during the deposition process. Besides the material use
667 and emission generations, energy consumption of CVD is another concern for environmental
668 justifications. To increase the material utilization efficiency and reduce the amount of waste,
669 optimization of the reaction process through establishing an optimal precursor supply pattern is
670 required. Likewise, the chemical reduction of GO mostly includes highly hazardous reducing
671 agents that are dangerous to the environment. Nevertheless, green synthesis strategies of
672 graphene have been developed recently by using bio-materials or non-toxic chemicals as
673 reducing agents, which are eco-friendly [156].

674 (2) *Graphene-based laminate coating*: The principal by-products for ALD coating process is
675 methane, a major greenhouse gas and has a global warming potential 25 times that of carbon
676 dioxide [157]. The material utilization efficiencies of precursors are reported below 20% in
677 ALD operations, which is mainly due to the limitation by the smaller working area compared

678 with the ALD reactor. In contrast, layer-by-layer assembly is considered as an environmentally
679 friendly process to ensure sustainable consumption and production of film materials.

680 (3) *Graphene-based nanocomposite coating*: Owing to growing environmental concerns on
681 emission of organic volatiles, waterborne polyurethane (WPU) has become an attractive
682 material for coating applications. To increase environmental friendliness and sustainability,
683 water is a tempting choice as an exfoliation medium, especially for WPU/graphene
684 nanocomposites. In addition, sustainable noncovalent modifiers are preferred to alleviate the
685 dispersion issues. Recently, graphene-based WPU nanocomposite coating has been prepared
686 by using a green, aqueous-only production route from graphite, showing great prospect in the
687 application of corrosion prevention [158].

688 By comparison of five key indicators for the present assessment on three different graphene-based
689 coatings, a radar plot is drawn in Fig. 12 whereby a preference score (1 = low, 2 = medium and 3 =
690 high) is assigned to each key indicator. The most promising graphene-based coating for
691 commercialization in anti-corrosion applications would be indicated by the highest total score. Based
692 on the ranking in this study, considering the comprehensive performance, graphene-based
693 nanocomposite coating exhibits the strongest potential for long-term stability, scalability, cost-
694 effectiveness, quality, and environmental sustainability, over to the other two types of graphene-based
695 coatings considered in this study, and therefore is optimal option for further research regarding anti-
696 corrosive performance of steel rebars.



697
698 **Fig. 12** A radar plot showing a comparison of comprehensive performance among three different graphene-based coatings.

699 4. Future prospects

700 Corrosion of structural steel and reinforcing steel rebar in concrete is a major issue for the stability,
701 integrity and service life of civil infrastructure. Corrosion of steel rebar in concrete, for example, can
702 lead to the cracking of concrete, spalling, and staining of the RCC infrastructure. Epoxy resins can be
703 adopted as anti-corrosive coatings in structural steel and rebar due to its crosslinking structures which
704 provide high adhesion and chemical resistance. However, epoxy-coated steel is brittle [57] and have
705 undergo pitting corrosion. Epoxy-coated steel rebar failure in a reinforced concrete structure was

706 identified in the early 1990s [159]. Another current industry practice is galvanized steel coated with a
707 layer of zinc, which is reported to have conflicting performance. One study reported that the threshold
708 level for initiating corrosion in galvanized rebar is 4 to 10 times higher than the threshold level for HR
709 steel rebar while another study reported that galvanized rebar have a slightly improved anti-corrosion
710 performance in severe chloride environments [160].

711 In comparison, graphene based anti-corrosive coating on steel rebar are examined. Nano layer thick
712 (single to multi-layer) pristine graphene coated steel [38–40,161] are reported to have up to 45 times
713 lower corrosion rate [38] compared to bare SS steel. Graphene composite based coating on steel with
714 0.8 to 110 μm uniform thickness [19,49,51,52,55] was reported to reduce the corrosion rate up to 10,000
715 times [53] compared to that of bare CR steel. The durability performance of steel rebar in concrete show
716 a significant improvement after multilayer electrostatic GO coating [44], and GO/CNT/epoxy based
717 composite coating [57]. The addition of graphene based coating on steel as well as complete coverage
718 of surface by the adherent layer plays important role for long-term durability of the coating [50]. Future
719 research direction of graphene-based anti-corrosive coating and other 2D materials-based coating are
720 presented in the section that follows.

721 **4.1. Graphene-based smart anti-corrosive coatings**

722 Advancement in nanotechnology and graphene-based anticorrosive coating is expected to pave a way
723 for the developments of effective multifunctional construction materials with smart properties. Based
724 on the assessment in this study, while graphene-based nanocomposite coating outperforms monolithic
725 and laminate coating in view of long-term protection, there remain some practical questions to be
726 solved. The long-term persistence of nanocomposite coating is still threatened by unexpected
727 mechanical damage due to repeated wear and tear and accidental cutting or scratching. A polymer's
728 durability and stability of the graphene based composite system warrants attention, particularly in a
729 high alkaline environment [44]. Other durability factors of concrete besides NaCl attack on steel rebar,
730 such as sulfate attack and carbonation [162] impact on graphene coated steel need in-depth
731 investigation. Development of smart composite coatings with self-sensing [163], and self-healing
732 [164,165], multifunctional capability (sensing, self-healing, repair, and restoration of functions) will be
733 a future direction.

734 To this end, the superior physicochemical properties of graphene enable it to play various functional
735 roles in different healing mechanisms, both intrinsic and extrinsic. Self-healing in construction materials
736 field referred to any process the materials recovers its performance after initial damage, such as strength,
737 density and permeability [166]. In terms of the intrinsic healing mechanism, where reversible chemical
738 bonds are dissociated and reconstructed by external stimulation to repair the material, graphene can not
739 only act as the centre of energy transfer and conversion to improve the efficiency of energy transfer,
740 but also carry functional groups to facilitate the construction of reversible chemical bonds [165].
741 Moreover, the thermal conductivity and photothermal/microwave conversion ability of graphene
742 combined afford the possibility for the multilevel healing in coating. On the other hand, for the extrinsic
743 healing coating, graphene is deemed as a promising inorganic nano-container to carry inhibitor
744 molecules, due to its large specific surface area and abundant active absorption sites on the surface. The
745 graphene-based nanocontainers possess lamellar morphology and can be applied to steel rebar ultra-
746 thin coatings with smart functionalities without affecting the stability. Both intrinsic and extrinsic self-
747 healing mechanisms represents the future development trend of self-healing graphene-based composite
748 anticorrosive coatings.

749 In addition, flexible graphene-based thin layer shows the ability of high sensitivity which can be applied
750 to measure electrical signals generated from small deformation [163], providing a viable means to strain
751 sensors smart coating on steel rebar. The graphene-based smart coated sensors with ultrafast response
752 could capture the time-dependent mechanical response through the coated steel rebar in the
753 infrastructure. The combination of thin coating, higher efficiency in anti-corrosion properties and
754 possibilities of these smart properties is expected to revolutionize steel rebar and structural steel
755 performance in the civil infrastructure industry.

756 **4.2. Anti-corrosive coating of 2D materials beyond graphene**

757 Graphene has been studied most for coating application among the other dense 2D nanostructure
758 materials, such as hexagonal boron nitride (hBN), molybdenum disulfide (MoS_2), and molybdenum
759 diselenide (MoSe_2), which show promising scope to develop nanoscale coating on steel with several
760 tuneable properties. Despite the great potential of graphene as anti-corrosive coatings, it is cathodic to
761 most metals and can promote corrosion at exposed graphene–metal interfaces owing to the galvanic
762 coupling. In that aspect, functionalization of graphene with nonconductive properties such as GO, and
763 the conjugation of all forms of graphene with insulating polymer and other 2D nanomaterials are more
764 suitable solutions for mitigating this issue and develop effective coating in steel surface.

765 In depth investigation on other 2D materials beyond graphene such as hBN, MoS_2 , and MoSe_2 is
766 required to explore for the development of next generation smart coatings. Hexagonal boron nitride
767 (hBN), for example, is a layered 2D electrical insulator (also called “white graphene”), can well resolve
768 the galvanic corrosion issues and has become an ideal coating material against corrosion. Considering
769 the similar hexagonal structure as graphene, hBN is also expected to have a high impermeability and
770 provide the barrier protection. In addition, it was reported that hBN coating could substantially reduce
771 the oxidation of metallic surfaces at extremely high temperatures owing to its exceptional thermal and
772 chemical stabilities [167]. Even under a range of abiotic (sulfuric acid and sodium sulfide) and biotic
773 (sulfate-reducing bacteria medium) sulfuric environments, atomically thin hBN layers can still
774 effectively inhibit the corrosion of the underlying copper [168]. Furthermore, hBN can be composited
775 with polymers to make hybrid paint, which was found to provide excellent protection of stainless steels
776 from marine corrosion when tested under a simulated seawater media [48]. Recently, the direct growth
777 of large-area, high-quality, uniform, and continuous h-BN coating on industry-relevant SS304 surfaces
778 has been realized by magnetic sputtering method, which may accelerate the progress of hBN nanofilm
779 applications in the industry [169]. It is envisaged that conformal coatings based on 2D materials and
780 their heterostructures will afford appealing routes to protect metals against aggressive environments
781 including thermal oxidation, microbial corrosion, and atmospheric corrosion [170,171]. Add to that, the
782 functionalized graphene could be combined with hBN to produce a thin layer coating for steel with cost
783 effective and multifunctional properties.

784

785 **5. Conclusions**

786 Reinforcement in concrete infrastructure exposed to corrosive environment is required to have high
787 anti-corrosive properties. Conventional epoxy and zinc coated steel rebar, in that aspect, have increasing
788 demand in the construction industry despite of their limitations and controversial performance in many
789 cases. Graphene-based anti-corrosive coating could be an effective solution in the development of next
790 generation steel rebar industry.

791 This review presents the progress on multiple sorts of graphene in the forms of monolithic, laminate,
792 and nanocomposite anti-corrosive coatings with a focus on steel applications. A clear picture of each
793 coating process is provided in a chronological discussion of anti-corrosion mechanism, preparation and
794 coating methods, and anti-corrosion performance. Despite the significant potential of graphene as
795 protective coatings, this study identifies the roadblocks and challenges that need to be addressed before
796 reaching market. The review also critically compares the three different graphene-based coating
797 systems with respect to long-term stability, scalability, cost-effectiveness, quality, and environmental
798 sustainability, leading to proposed recommendations on the future of research in the field of steel rebar
799 coating for civil infrastructure application. To summarize the key findings:

800 Graphene-based monolithic coating can be thinnest possible coating (nanoscale) with ultrahigh fracture
801 strength and fatigue life. The anti-corrosion mechanism lies in its impermeability to gases and liquids.
802 However, structural defects are inevitable for no matter CVD grown or solution processed graphene
803 films, which accelerate the corrosion of metals in the long term. The brittleness of graphene also makes
804 it vulnerable to scratches or cracks, easily resulting in an incomplete coating coverage on the substrate
805 surface. Furthermore, intrinsic corrugations and weak van der Waals interactions enable corrosive
806 molecules to diffuse, intercalate and penetrate at the interface, accounting for the short-term protection
807 as well.

808 In this regard, graphene-based laminate coatings being the combination of graphene with polymer or
809 ceramic in hybrid coatings provides a thicker and more robust corrosion barrier for the metal surface.
810 The layer-by-layer assembled structure with precise control of composition and thickness would be
811 more compact and ordered, efficiently suppressing the cohesive failure and affording a complete sealing
812 of metal surfaces. Furthermore, additional insulating protective layer aids to break the galvanic coupling
813 between graphene and metal substrate, which benefits the long-term anti-corrosion performance to meet
814 the industrial requirements. Nevertheless, the major concerns of the steel industry over using graphene-
815 based laminate as a corrosion inhibitor are related to the technical difficulties in layer-by-layer
816 assembly. For example, the demands of high throughput and quality for industrial-scale mechanical
817 transfer and stacking of graphene/polymer coating have not been fulfilled. Residual stress raises critical
818 issues in ALD layer that are detrimental to the stability and reliability of the laminate coating. More
819 concerns regarding the application of steel rebar with rough, nonuniform surfaces need to be addressed.

820 Generally, an optimal route to overcome many of these issues is to incorporate graphene into polymers
821 to produce the nanocomposite coating. Compared to graphene-based monolithic and laminate coating,
822 graphene-based nanocomposite coating, can be versatile, cost-effective, easily scalable with consistent
823 quality, much thicker, which is an efficient solution for steel surface corrosion protection. The
824 embedded graphene not only inhibits the penetration of corrosive substances (torturous effect), but also
825 retards the propagation of cracks (toughening mechanism). The resulting composite coating also
826 leverage the advantages of a polymer coating, such as the scratch-resistance and conformal adherence
827 to the substrate. The mature technology, detailed protocols and standard operating procedures for
828 polymer manufacturing and coating could be transferred to the production of nanocomposite coatings
829 on steel. In addition, considering the multifunctionality of graphene and extensive library of polymer
830 matrix, the nanocomposite coating will hold enormous potential in adaptation to a broad spectrum of
831 applications. To fully unleash the potential, strategies to increase the dispersion, interface bonding, and
832 alignment of graphene in polymer matrix are required. The concentration of graphene in the polymer
833 nanocomposite should be selected considering the fact that the agglomeration effect of nanomaterials
834 could occurs at low filler concentration compromising the excellent water barrier properties. More
835 efforts should be directed toward developing green and environmentally friendly modification methods,
836 to minimize pollutions and health hazards. In addition, from the scientific perspective, optimized design

837 of nanocomposite coating requires deeper understanding of the specific materials and interfacial
838 interactions, especially detailed structure-property-function relationships. Computational tools are
839 hence necessary to capture the physics and chemistry of the nanomaterials as well as their interfaces
840 during the deformation and failure process. Predictive multiscale modelling can leverage quantum
841 mechanics calculations (e.g. density functional theory) to describe the electronic structure and coupling
842 of individual building blocks, as well as larger scale models to understand the structure of the materials
843 up to the continuum level. The integration of theoretical modelling, numerical simulations and
844 experimentation is instrumental to develop a multiscale structure-property paradigm that guides an
845 accurate design of high-performance nanocomposite coatings.

846

847 **CRedit author statement**

848 **Tanvir Qureshi:** Conceptualization, Methodology, Investigation, Writing - Original Draft,
849 Visualization. **Guorui Wang:** Conceptualization, Methodology, Investigation, Writing - Original Draft,
850 Visualization. **Sankha Mukherjee:** Writing - Original Draft. **Md Akibul Islam:** Writing - Original
851 Draft. **Tobin Filleter:** Writing - Review & Editing, Funding acquisition. **Chandra V. Singh:** Writing
852 - Review & Editing, Funding acquisition. and **Daman K. Panesar:** Writing - Review & Editing,
853 Funding acquisition.

854 **Declaration of competing interest**

855 The authors declare that they have no known competing financial interests or personal
856 relationships that could have appeared to influence the work reported in this paper.

857

858 **Acknowledgements**

859 Tanvir Qureshi and Guorui Wang contributed equally to this work. The authors are grateful for support
860 from the University of Toronto Dean's Strategic Fund for the U of T Centre for 2D Materials, and
861 funding from Natural Sciences and Engineering Research Council of Canada (NSERC). The authors
862 are also grateful for Tanvir Qureshi's Vice-Chancellor's Early Career Researcher Development Award
863 (VC ECR) from UWE Bristol.

864

865 **References**

- 866 [1] A. Poursaee, Corrosion of steel in concrete structures, in: Corros. Steel Concr. Struct., Elsevier
867 Inc., 2016: pp. 19–33. <https://doi.org/10.1016/B978-1-78242-381-2.00002-X>.
- 868 [2] G. Koch, J. Varney, N. Thompson, O. Moghissi, M. Gould, J. Payer, International Measures of
869 Prevention, Application, and Economics of Corrosion Technologies Study, 2016.
870 [http://impact.nace.org/documents/Nace-International-](http://impact.nace.org/documents/Nace-International-Report.pdf%0Apapers3://publication/uuid/9784056A-47E3-4988-8D70-B6763CF35EBF)
871 [Report.pdf%0Apapers3://publication/uuid/9784056A-47E3-4988-8D70-B6763CF35EBF](http://impact.nace.org/documents/Nace-International-Report.pdf%0Apapers3://publication/uuid/9784056A-47E3-4988-8D70-B6763CF35EBF)
872 (accessed May 6, 2021).
- 873 [3] M.P.H. Gerhardus H. Koch, and N.G.T.Y.P.V.J.H.P. Brongers, Corrosion costs and
874 preventive strategies in the United States, 2002. [papers2://publication/uuid/4D469A9D-07D6-](papers2://publication/uuid/4D469A9D-07D6-4543-B217-3A15873793CF)
875 [4543-B217-3A15873793CF](papers2://publication/uuid/4D469A9D-07D6-4543-B217-3A15873793CF) (accessed May 23, 2021).
- 876 [4] T. Zafeiropoulou, E. Rakanta, G. Batis, Performance evaluation of organic coatings against
877 corrosion in reinforced cement mortars, Prog. Org. Coatings. 72 (2011) 175–180.

- 878 <https://doi.org/10.1016/J.PORGCOAT.2011.04.005>.
- 879 [5] J.P. Broomfield, Corrosion of Steel in Concrete: Understanding, Investigation and Repair,
880 Second Edition, E FN SPOK. (2006) 296.
881 [http://books.google.co.uk/books/about/Corrosion_of_Steel_in_Concrete.html?id=kjTzl9NVHs](http://books.google.co.uk/books/about/Corrosion_of_Steel_in_Concrete.html?id=kjTzl9NVHsQC&pgis=1)
882 [QC&pgis=1](http://books.google.co.uk/books/about/Corrosion_of_Steel_in_Concrete.html?id=kjTzl9NVHsQC&pgis=1) (accessed February 16, 2021).
- 883 [6] Jahresbericht 1991 der Arbeitsgemeinschaft Korrosion e.V. (AGK), Mater. Corros. 43 (1992)
884 224–257. <https://doi.org/10.1002/maco.19920430509>.
- 885 [7] M. Moreno, W. Morris, M.G. Alvarez, G.S. Duffó, Corrosion of reinforcing steel in simulated
886 concrete pore solutions effect of carbonation and chloride content, Corros. Sci. 46 (2004)
887 2681–2699. <https://doi.org/10.1016/j.corsci.2004.03.013>.
- 888 [8] O. ur Rahman, M. Kashif, S. Ahmad, Nanoferrite dispersed waterborne epoxy-acrylate:
889 Anticorrosive nanocomposite coatings, Prog. Org. Coatings. 80 (2015) 77–86.
890 <https://doi.org/10.1016/J.PORGCOAT.2014.11.023>.
- 891 [9] P.A. Sørensen, S. Kiil, K. Dam-Johansen, C.E. Weinell, Anticorrosive coatings: a review, J.
892 Coatings Technol. Res. 6 (2009) 135–176. <https://doi.org/10.1007/s11998-008-9144-2>.
- 893 [10] Y. Qing, C. Yang, C. Hu, Y. Zheng, C. Liu, A facile method to prepare superhydrophobic
894 fluorinated polysiloxane/ZnO nanocomposite coatings with corrosion resistance, Appl. Surf.
895 Sci. 326 (2015) 48–54. <https://doi.org/10.1016/J.APSUSC.2014.11.100>.
- 896 [11] S. Kango, S. Kalia, A. Celli, J. Njuguna, Y. Habibi, R. Kumar, Surface modification of
897 inorganic nanoparticles for development of organic–inorganic nanocomposites—A review,
898 Prog. Polym. Sci. 38 (2013) 1232–1261.
899 <https://doi.org/10.1016/J.PROGPOLYMSCI.2013.02.003>.
- 900 [12] S.K. Dhoke, A.S. Khanna, T.J.M. Sinha, “Effect of nano-ZnO particles on the corrosion
901 behavior of alkyd-based waterborne coatings,” Prog. Org. Coatings. 64 (2009) 371–382.
902 <https://doi.org/10.1016/J.PORGCOAT.2008.07.023>.
- 903 [13] S.K. Dhoke, T.J. Mangal Sinha, A.S. Khanna, Effect of nano-Al₂O₃ particles on the corrosion
904 behavior of alkyd based waterborne coatings, J. Coatings Technol. Res. 6 (2009) 353–368.
905 <https://doi.org/10.1007/s11998-008-9127-3>.
- 906 [14] Y. Chen, S. Zhou, H. Yang, L. Wu, Structure and properties of polyurethane/nanosilica
907 composites, J. Appl. Polym. Sci. 95 (2005) 1032–1039. <https://doi.org/10.1002/app.21180>.
- 908 [15] X. Shi, T.A. Nguyen, Z. Suo, Y. Liu, R. Avci, Effect of nanoparticles on the anticorrosion and
909 mechanical properties of epoxy coating, Surf. Coatings Technol. 204 (2009) 237–245.
910 <https://doi.org/10.1016/J.SURFCOAT.2009.06.048>.
- 911 [16] F. Tang, Steel Rebar Coatings for Concrete Structures, Struct. Mag. (2016).
912 <https://www.structuremag.org/?p=10047> (accessed February 17, 2021).
- 913 [17] A. Krishnamurthy, V. Gadhamshetty, R. Mukherjee, B. Natarajan, O. Eksik, S. Ali Shojaee,
914 D.A. Lucca, W. Ren, H.M. Cheng, N. Koratkar, Superiority of graphene over polymer
915 coatings for prevention of microbially induced corrosion, Sci. Rep. 5 (2015) 1–12.
916 <https://doi.org/10.1038/srep13858>.
- 917 [18] D. Prasai, J.C. Tuberquia, R.R. Harl, G.K. Jennings, K.I. Bolotin, Graphene: Corrosion-
918 inhibiting coating, ACS Nano. 6 (2012) 1102–1108. <https://doi.org/10.1021/nn203507y>.
- 919 [19] G. Christopher, M. Anbu Kulandainathan, G. Harichandran, Comparative study of effect of
920 corrosion on mild steel with waterborne polyurethane dispersion containing graphene oxide
921 versus carbon black nanocomposites, Prog. Org. Coatings. 89 (2015) 199–211.
922 <https://doi.org/10.1016/J.PORGCOAT.2015.09.022>.
- 923 [20] G. Cui, Z. Bi, R. Zhang, J. Liu, X. Yu, Z. Li, A comprehensive review on graphene-based anti-
924 corrosive coatings, Chem. Eng. J. 373 (2019) 104–121.
- 925 [21] C. Lee, X. Wei, J.W. Kysar, J. Hone, Measurement of the elastic properties and intrinsic

- 926 strength of monolayer graphene, *Science* (80-.). (2008).
 927 <https://doi.org/10.1126/science.1157996>.
- 928 [22] T. Cui, S. Mukherjee, P.M. Sudeep, G. Colas, F. Najafi, J. Tam, P.M. Ajayan, C.V. Singh, Y.
 929 Sun, T. Filleter, Fatigue of graphene, *Nat. Mater.* (2020). [https://doi.org/10.1038/s41563-019-](https://doi.org/10.1038/s41563-019-0586-y)
 930 [0586-y](https://doi.org/10.1038/s41563-019-0586-y).
- 931 [23] C. Lee, Q. Li, W. Kalb, X.Z. Liu, H. Berger, R.W. Carpick, J. Hone, Frictional characteristics
 932 of atomically thin sheets, *Science* (80-.). (2010). <https://doi.org/10.1126/science.1184167>.
- 933 [24] T. Arif, G. Colas, T. Filleter, Effect of Humidity and Water Intercalation on the Tribological
 934 Behavior of Graphene and Graphene Oxide, *ACS Appl. Mater. Interfaces.* (2018).
 935 <https://doi.org/10.1021/acsami.8b03776>.
- 936 [25] T.S. Qureshi, D.K. Panesar, Nano reinforced cement paste composite with functionalized
 937 graphene and pristine graphene nanoplatelets, *Compos. Part B Eng.* 197 (2020) 108063.
 938 <https://doi.org/10.1016/j.compositesb.2020.108063>.
- 939 [26] T.S. Qureshi, D.K. Panesar, Impact of graphene oxide and highly reduced graphene oxide on
 940 cement based composites, *Constr. Build. Mater.* 206 (2019) 71–83.
 941 <https://doi.org/10.1016/j.conbuildmat.2019.01.176>.
- 942 [27] A.A. Balandin, S. Ghosh, W. Bao, I. Calizo, D. Teweldebrhan, F. Miao, C.N. Lau, Superior
 943 thermal conductivity of single-layer graphene, *Nano Lett.* 8 (2008) 902–907.
 944 <https://doi.org/10.1021/nl0731872>.
- 945 [28] K.S. Kim, Y. Zhao, H. Jang, S.Y. Lee, J.M. Kim, K.S. Kim, J.H. Ahn, P. Kim, J.Y. Choi, B.H.
 946 Hong, Large-scale pattern growth of graphene films for stretchable transparent electrodes,
 947 *Nature.* 457 (2009) 706–710. <https://doi.org/10.1038/nature07719>.
- 948 [29] M. Owais, J. Zhao, A. Imani, G. Wang, H. Zhang, Z. Zhang, Synergetic effect of hybrid fillers
 949 of boron nitride, graphene nanoplatelets, and short carbon fibers for enhanced thermal
 950 conductivity and electrical resistivity of epoxy nanocomposites, *Compos. Part A Appl. Sci.*
 951 *Manuf.* 117 (2019) 11–22. <https://doi.org/10.1016/j.compositesa.2018.11.006>.
- 952 [30] J. Hu, Y. Ji, Y. Shi, F. Hui, H.L. Duan, A Review on the use of Graphene as a Protective
 953 Coating against Corrosion, *Ann. Mater. Sci. Eng.* 1 (2014) 16.
 954 www.austinpublishinggroup.com.
- 955 [31] D.S. Chauhan, M.A. Quraishi, K.R. Ansari, T.A. Saleh, Graphene and graphene oxide as new
 956 class of materials for corrosion control and protection: Present status and future scenario, *Prog.*
 957 *Org. Coatings.* 147 (2020) 105741. <https://doi.org/10.1016/J.PORGCOAT.2020.105741>.
- 958 [32] R. Ding, W. Li, X. Wang, T. Gui, B. Li, P. Han, H. Tian, A. Liu, X. Wang, X. Liu, X. Gao, W.
 959 Wang, L. Song, A brief review of corrosion protective films and coatings based on graphene
 960 and graphene oxide, *J. Alloys Compd.* 764 (2018) 1039–1055.
 961 <https://doi.org/10.1016/j.jallcom.2018.06.133>.
- 962 [33] M.J. Nine, M.A. Cole, D.N.H. Tran, D. Losic, Graphene: A multipurpose material for
 963 protective coatings, *J. Mater. Chem. A.* 3 (2015) 12580–12602.
 964 <https://doi.org/10.1039/c5ta01010a>.
- 965 [34] N.H. Othman, M. Che Ismail, M. Mustapha, N. Sallih, K.E. Kee, R. Ahmad Jaal, Graphene-
 966 based polymer nanocomposites as barrier coatings for corrosion protection, *Prog. Org.*
 967 *Coatings.* 135 (2019) 82–99. <https://doi.org/10.1016/j.porgcoat.2019.05.030>.
- 968 [35] M. Bethencourt, F.J. Botana, J.J. Calvino, M. Marcos, M.A. Rodríguez-Chacón, Graphene
 969 based materials and their composites as coatings, *Corros. Sci.* 13 (1998) 1803–1819.
 970 <https://doi.org/10.3144/expresspolymlett.2013.72>.
- 971 [36] A. Gergely, A review on corrosion protection with single-layer, multilayer, and composites of
 972 graphene, *Corros. Rev.* 36 (2018) 155–225. <https://doi.org/10.1515/corrrev-2017-0016>.
- 973 [37] R.S. Weatherup, L. D’Arsié, A. Cabrero-Vilatela, S. Caneva, R. Blume, J. Robertson, R.

- 974 Schloegl, S. Hofmann, Long-Term Passivation of Strongly Interacting Metals with Single-
975 Layer Graphene, *J. Am. Chem. Soc.* 137 (2015) 14358–14366.
976 <https://doi.org/10.1021/jacs.5b08729>.
- 977 [38] N.-W. Pu, G.-N. Shi, Y.-M. Liu, X. Sun, J.-K. Chang, C.-L. Sun, M.-D. Ger, C.-Y. Chen, P.-C.
978 Wang, Y.-Y. Peng, C.-H. Wu, S. Lawes, Graphene grown on stainless steel as a high-
979 performance and ecofriendly anti-corrosion coating for polymer electrolyte membrane fuel cell
980 bipolar plates, *J. Power Sources.* 282 (2015) 248–256.
981 <https://doi.org/10.1016/J.JPOWSOUR.2015.02.055>.
- 982 [39] M. Zhu, Z. Du, Z. Yin, W. Zhou, Z. Liu, S.H. Tsang, E.H.T. Teo, Low-Temperature in Situ
983 Growth of Graphene on Metallic Substrates and Its Application in Anticorrosion, *ACS Appl.*
984 *Mater. Interfaces.* 8 (2016) 502–510. <https://doi.org/10.1021/acsami.5b09453>.
- 985 [40] X. Ye, Z. Lin, H. Zhang, H. Zhu, Z. Liu, M. Zhong, Protecting carbon steel from corrosion by
986 laser in situ grown graphene films, *Carbon N. Y.* 94 (2015) 326–334.
987 <https://doi.org/10.1016/J.CARBON.2015.06.080>.
- 988 [41] S. Mayavan, T. Siva, S. Sathiyarayanan, Graphene ink as a corrosion inhibiting blanket for
989 iron in an aggressive chloride environment, *RSC Adv.* (2013).
990 <https://doi.org/10.1039/c3ra43931c>.
- 991 [42] M. Bagherzadeh, Z.S. Ghahfarokhi, E.G. Yazdi, Electrochemical and surface evaluation of the
992 anti-corrosion properties of reduced graphene oxide, *RSC Adv.* (2016).
993 <https://doi.org/10.1039/c5ra26948b>.
- 994 [43] J.A. Quezada-Rentería, L.F. Cházaro-Ruiz, J.R. Rangel-Mendez, Synthesis of reduced
995 graphene oxide (rGO) films onto carbon steel by cathodic electrophoretic deposition:
996 Anticorrosive coating, *Carbon N. Y.* 122 (2017) 266–275.
997 <https://doi.org/10.1016/j.carbon.2017.06.074>.
- 998 [44] Y. Zhu, Z. Zhang, Investigation of the anticorrosion layer of reinforced steel based on
999 graphene oxide in simulated concrete pore solution with 3 wt.% NaCl, *J. Build. Eng.* 44 (2021)
1000 103302. <https://doi.org/10.1016/J.JOBE.2021.103302>.
- 1001 [45] J. Mondal, A. Marques, L. Aarik, J. Kozlova, A. Simões, V. Sammelselg, Development of a
1002 thin ceramic-graphene nanolaminate coating for corrosion protection of stainless steel, *Corros.*
1003 *Sci.* 105 (2016) 161–169. <https://doi.org/10.1016/J.CORSCI.2016.01.013>.
- 1004 [46] H. Zhang, S. Ren, J. Pu, Q. Xue, Barrier mechanism of multilayers graphene coated copper
1005 against atomic oxygen irradiation, *Appl. Surf. Sci.* 444 (2018) 28–35.
1006 <https://doi.org/10.1016/J.APSUSC.2018.03.026>.
- 1007 [47] Y.-P. Hsieh, M. Hofmann, K.-W. Chang, J.G. Jhu, Y.-Y. Li, K.Y. Chen, C.C. Yang, W.-S.
1008 Chang, L.-C. Chen, Complete Corrosion Inhibition through Graphene Defect Passivation, *ACS*
1009 *Nano.* 8 (2014) 443–448. <https://doi.org/10.1021/nn404756q>.
- 1010 [48] E. Husain, T.N. Narayanan, J.J. Taha-Tijerina, S. Vinod, R. Vajtai, P.M. Ajayan, Marine
1011 corrosion protective coatings of hexagonal boron nitride thin films on stainless steel, *ACS*
1012 *Appl. Mater. Interfaces.* 5 (2013) 4129–4135. <https://doi.org/10.1021/am400016y>.
- 1013 [49] K.S. Aneja, S. Bohm, A.S. Khanna, H.L.M. Bohm, Graphene based anticorrosive coatings for
1014 Cr(vi) replacement, *Nanoscale.* 7 (2015) 17879–17888.
1015 <https://doi.org/10.1039/C5NR04702A>.
- 1016 [50] K.S. Aneja, H.L.M. Böhm, A.S. Khanna, S. Böhm, Functionalised graphene as a barrier
1017 against corrosion, *FlatChem.* 1 (2017) 11–19. <https://doi.org/10.1016/J.FLATC.2016.08.003>.
- 1018 [51] C. Liu, S. Qiu, P. Du, H. Zhao, L. Wang, An ionic liquid–graphene oxide hybrid nanomaterial:
1019 synthesis and anticorrosive applications, *Nanoscale.* 10 (2018) 8115–8124.
1020 <https://doi.org/10.1039/C8NR01890A>.
- 1021 [52] Y.N. Singhababu, B. Sivakumar, J.K. Singh, H. Bapari, A.K. Pramanick, R.K. Sahu, Efficient
1022 anti-corrosive coating of cold-rolled steel in a seawater environment using an oil-based

- 1023 graphene oxide ink, *Nanoscale*. 7 (2015) 8035–8047. <https://doi.org/10.1039/C5NR01453K>.
- 1024 [53] Y.N. Singhababu, B. Sivakumar, S.K. Choudhary, S. Das, R.K. Sahu, Corrosion-protective
1025 reduced graphene oxide coated cold rolled steel prepared using industrial setup: A study of
1026 protocol feasibility for commercial production, *Surf. Coatings Technol.* 349 (2018) 119–132.
1027 <https://doi.org/10.1016/J.SURFCOAT.2018.05.046>.
- 1028 [54] C.-H. Chang, T.-C. Huang, C.-W. Peng, T.-C. Yeh, H.-I. Lu, W.-I. Hung, C.-J. Weng, T.-I.
1029 Yang, J.-M. Yeh, Novel anticorrosion coatings prepared from polyaniline/graphene
1030 composites, *Carbon N. Y.* 50 (2012) 5044–5051.
1031 <https://doi.org/10.1016/J.CARBON.2012.06.043>.
- 1032 [55] K.-C. Chang, M.-H. Hsu, H.-I. Lu, M.-C. Lai, P.-J. Liu, C.-H. Hsu, W.-F. Ji, T.-L. Chuang, Y.
1033 Wei, J.-M. Yeh, W.-R. Liu, Room-temperature cured hydrophobic epoxy/graphene composites
1034 as corrosion inhibitor for cold-rolled steel, *Carbon N. Y.* 66 (2014) 144–153.
1035 <https://doi.org/10.1016/J.CARBON.2013.08.052>.
- 1036 [56] X. Li, P. Bandyopadhyay, M. Guo, N.H. Kim, J.H. Lee, Enhanced gas barrier and
1037 anticorrosion performance of boric acid induced cross-linked poly(vinyl alcohol-co-
1038 ethylene)/graphene oxide film, *Carbon N. Y.* 133 (2018) 150–161.
1039 <https://doi.org/10.1016/J.CARBON.2018.03.036>.
- 1040 [57] N. Sharma, S. Sharma, S.K. Sharma, R.L. Mahajan, R. Mehta, Evaluation of corrosion
1041 inhibition capability of graphene modified epoxy coatings on reinforcing bars in concrete,
1042 *Constr. Build. Mater.* 322 (2022) 126495.
1043 <https://doi.org/10.1016/J.CONBUILDMAT.2022.126495>.
- 1044 [58] V. Berry, Impermeability of graphene and its applications, *Carbon N. Y.* 62 (2013) 1–10.
1045 <https://doi.org/10.1016/j.carbon.2013.05.052>.
- 1046 [59] J.S. Bunch, S.S. Verbridge, J.S. Alden, A.M. Van Der Zande, J.M. Parpia, H.G. Craighead,
1047 P.L. McEuen, Impermeable atomic membranes from graphene sheets, *Nano Lett.* (2008).
1048 <https://doi.org/10.1021/nl801457b>.
- 1049 [60] P.Z. Sun, Q. Yang, W.J. Kuang, Y. V. Stebunov, W.Q. Xiong, J. Yu, R.R. Nair, M.I.
1050 Katsnelson, S.J. Yuan, I. V. Grigorieva, M. Lozada-Hidalgo, F.C. Wang, A.K. Geim, Limits
1051 on gas impermeability of graphene, *Nature*. (2020). [https://doi.org/10.1038/s41586-020-2070-](https://doi.org/10.1038/s41586-020-2070-x)
1052 [x](https://doi.org/10.1038/s41586-020-2070-x).
- 1053 [61] J.S. Qi, J.Y. Huang, J. Feng, D.N. Shi, J. Li, The possibility of chemically inert, graphene-
1054 based all-carbon electronic devices with 0.8 eV gap, *ACS Nano*. (2011).
1055 <https://doi.org/10.1021/nn102322s>.
- 1056 [62] L. Lin, B. Deng, J. Sun, H. Peng, Z. Liu, Bridging the Gap between Reality and Ideal in
1057 Chemical Vapor Deposition Growth of Graphene, *Chem. Rev.* 118 (2018) 9281–9343.
1058 <https://doi.org/10.1021/acs.chemrev.8b00325>.
- 1059 [63] L. Camilli, F. Yu, A. Cassidy, L. Hornekær, P. Bøggild, Challenges for continuous graphene
1060 as a corrosion barrier, *2D Mater.* 6 (2019) 022002. <https://doi.org/10.1088/2053-1583/ab04d4>.
- 1061 [64] D. Li, M.B. Müller, S. Gilje, R.B. Kaner, G.G. Wallace, Processable aqueous dispersions of
1062 graphene nanosheets, *Nat. Nanotechnol.* (2008). <https://doi.org/10.1038/nnano.2007.451>.
- 1063 [65] Y. Hernandez, V. Nicolosi, M. Lotya, F.M. Blighe, Z. Sun, S. De, I.T. McGovern, B. Holland,
1064 M. Byrne, Y.K. Gun'ko, J.J. Boland, P. Niraj, G. Duesberg, S. Krishnamurthy, R. Goodhue, J.
1065 Hutchison, V. Scardaci, A.C. Ferrari, J.N. Coleman, High-yield production of graphene by
1066 liquid-phase exfoliation of graphite, *Nat. Nanotechnol.* (2008).
1067 <https://doi.org/10.1038/nnano.2008.215>.
- 1068 [66] K.R. Paton, E. Varrla, C. Backes, R.J. Smith, U. Khan, A. O'Neill, C. Boland, M. Lotya, O.M.
1069 Istrate, P. King, T. Higgins, S. Barwich, P. May, P. Puczkarski, I. Ahmed, M. Moebius, H.
1070 Pettersson, E. Long, J. Coelho, S.E. O'Brien, E.K. McGuire, B.M. Sanchez, G.S. Duesberg, N.
1071 McEvoy, T.J. Pennycook, C. Downing, A. Crossley, V. Nicolosi, J.N. Coleman, Scalable

- 1072 production of large quantities of defect-free few-layer graphene by shear exfoliation in liquids,
1073 *Nat. Mater.* (2014). <https://doi.org/10.1038/nmat3944>.
- 1074 [67] E.S. Polsen, D.Q. McNerny, B. Viswanath, S.W. Pattinson, A. John Hart, High-speed roll-to-
1075 roll manufacturing of graphene using a concentric tube CVD reactor, *Sci. Rep.* (2015).
1076 <https://doi.org/10.1038/srep10257>.
- 1077 [68] L. Liu, Z. Shen, M. Yi, X. Zhang, S. Ma, A green, rapid and size-controlled production of
1078 high-quality graphene sheets by hydrodynamic forces, *RSC Adv.* (2014).
1079 <https://doi.org/10.1039/c4ra05635c>.
- 1080 [69] J.H. Park, J.M. Park, Electrophoretic deposition of graphene oxide on mild carbon steel for
1081 anti-corrosion application, *Surf. Coatings Technol.* 254 (2014) 167–174.
1082 <https://doi.org/10.1016/j.surfcoat.2014.06.007>.
- 1083 [70] Y. Su, V.G. Kravets, S.L. Wong, J. Waters, A.K. Geim, R.R. Nair, Impermeable barrier films
1084 and protective coatings based on reduced graphene oxide, *Nat. Commun.* 5 (2014) 1–5.
1085 <https://doi.org/10.1038/ncomms5843>.
- 1086 [71] D. Kang, J.Y. Kwon, H. Cho, J.H. Sim, H.S. Hwang, C.S. Kim, Y.J. Kim, R.S. Ruoff, H.S.
1087 Shin, Oxidation resistance of iron and copper foils coated with reduced graphene oxide
1088 multilayers, *ACS Nano.* 6 (2012) 7763–7769. <https://doi.org/10.1021/nn3017316>.
- 1089 [72] L. Wang, J.J. Travis, A.S. Cavanagh, X. Liu, S.P. Koenig, P.Y. Huang, S.M. George, J.S.
1090 Bunch, Ultrathin oxide films by atomic layer deposition on graphene, *Nano Lett.* (2012).
1091 <https://doi.org/10.1021/nl3014956>.
- 1092 [73] H. Caliskan, P. Panjan, C. Kurbanoglu, Hard Coatings on Cutting Tools and Surface Finish, in:
1093 *Compr. Mater. Finish.*, 2017. <https://doi.org/10.1016/B978-0-12-803581-8.09178-5>.
- 1094 [74] Y. Kubota, K. Watanabe, O. Tsuda, T. Taniguchi, Deep ultraviolet light-emitting hexagonal
1095 boron nitride synthesized at atmospheric pressure, *Science* (80-.). (2007).
1096 <https://doi.org/10.1126/science.1144216>.
- 1097 [75] K. Yan, H.W. Lee, T. Gao, G. Zheng, H. Yao, H. Wang, Z. Lu, Y. Zhou, Z. Liang, Z. Liu, S.
1098 Chu, Y. Cui, Ultrathin two-dimensional atomic crystals as stable interfacial layer for
1099 improvement of lithium metal anode, *Nano Lett.* (2014). <https://doi.org/10.1021/nl503125u>.
- 1100 [76] G. Wang, Z. Dai, J. Xiao, S.Z. Feng, C. Weng, L. Liu, Z. Xu, R. Huang, Z. Zhang, Bending of
1101 Multilayer van der Waals Materials, *Phys. Rev. Lett.* (2019).
1102 <https://doi.org/10.1103/PhysRevLett.123.116101>.
- 1103 [77] S.M. George, Atomic layer deposition: An overview, *Chem. Rev.* 110 (2010) 111–131.
1104 <https://doi.org/10.1021/cr900056b>.
- 1105 [78] C. Cao, S. Mukherjee, J. Liu, B. Wang, M. Amirmaleki, Z. Lu, J.Y. Howe, D. Perovic, X. Sun,
1106 C.V. Singh, Y. Sun, T. Filleter, Role of graphene in enhancing the mechanical properties of
1107 TiO₂/graphene heterostructures, *Nanoscale.* (2017). <https://doi.org/10.1039/c7nr03049e>.
- 1108 [79] M. Amirmaleki, T. Cui, Y. Zhao, J. Tam, A. Goel, Y. Sun, X. Sun, T. Filleter, Fracture and
1109 Fatigue of Al₂O₃-Graphene Nanolayers, *Nano Lett.* 21 (2021) 437–444.
1110 <https://doi.org/10.1021/acs.nanolett.0c03868>.
- 1111 [80] R.W. Johnson, A. Hultqvist, S.F. Bent, A brief review of atomic layer deposition: From
1112 fundamentals to applications, *Mater. Today.* 17 (2014) 236–246.
1113 <https://doi.org/10.1016/j.mattod.2014.04.026>.
- 1114 [81] K. Kim, H.B.R. Lee, R.W. Johnson, J.T. Tanskanen, N. Liu, M.G. Kim, C. Pang, C. Ahn, S.F.
1115 Bent, Z. Bao, Selective metal deposition at graphene line defects by atomic layer deposition,
1116 *Nat. Commun.* 5 (2014). <https://doi.org/10.1038/ncomms5781>.
- 1117 [82] X. Wang, S.M. Tabakman, H. Dai, Atomic layer deposition of metal oxides on pristine and
1118 functionalized graphene, *J. Am. Chem. Soc.* (2008). <https://doi.org/10.1021/ja8023059>.
- 1119 [83] J. Lipton, G.M. Weng, J.A. Röhr, H. Wang, A.D. Taylor, Layer-by-Layer Assembly of Two-

- 1120 Dimensional Materials: Meticulous Control on the Nanoscale, *Matter*. (2020).
 1121 <https://doi.org/10.1016/j.matt.2020.03.012>.
- 1122 [84] T. Lee, S.H. Min, M. Gu, Y.K. Jung, W. Lee, J.U. Lee, D.G. Seong, B.S. Kim, Layer-by-Layer
 1123 Assembly for Graphene-Based Multilayer Nanocomposites: Synthesis and Applications,
 1124 *Chem. Mater.* (2015). <https://doi.org/10.1021/acs.chemmater.5b00491>.
- 1125 [85] K. Hu, D.D. Kulkarni, I. Choi, V. V. Tsukruk, Graphene-polymer nanocomposites for
 1126 structural and functional applications, *Prog. Polym. Sci.* (2014).
 1127 <https://doi.org/10.1016/j.progpolymsci.2014.03.001>.
- 1128 [86] Q. Wu, W. Wongwiriyan, J.H. Park, S. Park, S.J. Jung, T. Jeong, S. Lee, Y.H. Lee, Y.J.
 1129 Song, In situ chemical vapor deposition of graphene and hexagonal boron nitride
 1130 heterostructures, *Curr. Appl. Phys.* (2016). <https://doi.org/10.1016/j.cap.2016.04.024>.
- 1131 [87] K.S. Novoselov, A. Mishchenko, A. Carvalho, A.H. Castro Neto, 2D materials and van der
 1132 Waals heterostructures, *Science* (80-). (2016). <https://doi.org/10.1126/science.aac9439>.
- 1133 [88] R. Frisenda, E. Navarro-Moratalla, P. Gant, D. Pérez De Lara, P. Jarillo-Herrero, R. V.
 1134 Gorbachev, A. Castellanos-Gomez, Recent progress in the assembly of nanodevices and van
 1135 der Waals heterostructures by deterministic placement of 2D materials, *Chem. Soc. Rev.*
 1136 (2018). <https://doi.org/10.1039/c7cs00556c>.
- 1137 [89] S. Fan, Q.A. Vu, M.D. Tran, S. Adhikari, Y.H. Lee, Transfer assembly for two-dimensional
 1138 van der Waals heterostructures, *2D Mater.* (2020). <https://doi.org/10.1088/2053-1583/ab7629>.
- 1139 [90] P. Liu, Z. Jin, G. Katsukis, L.W. Drahushuk, S. Shimizu, C.J. Shih, E.D. Wetzel, J.K. Taggart-
 1140 Scarff, B. Qing, K.J. Van Vliet, R. Li, B.L. Wardle, M.S. Strano, Layered and scrolled
 1141 nanocomposites with aligned semi-infinite graphene inclusions at the platelet limit, *Science*
 1142 (80-). (2016). <https://doi.org/10.1126/science.aaf4362>.
- 1143 [91] F. Yu, L. Camilli, T. Wang, D.M.A. Mackenzie, M. Curioni, R. Akid, P. Bøggild, Complete
 1144 long-term corrosion protection with chemical vapor deposited graphene, *Carbon N. Y.* 132
 1145 (2018) 78–84. <https://doi.org/10.1016/j.carbon.2018.02.035>.
- 1146 [92] S. Vandana, V. Kochat, J. Lee, V. Varshney, S. Yazdi, J. Shen, S. Kosolwattana, S. Vinod, R.
 1147 Vajtai, A.K. Roy, C.S. Tiwary, P.M. Ajayan, 2D Heterostructure coatings of hBN-MoS2
 1148 layers for corrosion resistance, *J. Phys. D. Appl. Phys.* 50 (2017) aa5001.
 1149 <https://doi.org/10.1088/1361-6463/aa5001>.
- 1150 [93] G. Wang, L. Liu, Z. Zhang, Interface mechanics in carbon nanomaterials-based
 1151 nanocomposites, *Compos. Part A Appl. Sci. Manuf.* (2021).
 1152 <https://doi.org/10.1016/j.compositesa.2020.106212>.
- 1153 [94] G. Wang, L. Liu, Z. Dai, Q. Liu, H. Miao, Z. Zhang, Biaxial compressive behavior of
 1154 embedded monolayer graphene inside flexible poly (methyl methacrylate) matrix, *Carbon N.*
 1155 *Y.* (2015). <https://doi.org/10.1016/j.carbon.2015.01.022>.
- 1156 [95] Y. Zhang, L. Liu, B. Sun, G. Wang, Z. Zhang, Preparation of lipophilic graphene oxide
 1157 derivatives via a concise route and its mechanical reinforcement in thermoplastic polyurethane,
 1158 *Compos. Sci. Technol.* 134 (2016) 36–42. <https://doi.org/10.1016/j.compscitech.2016.07.027>.
- 1159 [96] L.S. Walker, V.R. Marotto, M.A. Rafiee, N. Koratkar, E.L. Corral, Toughening in graphene
 1160 ceramic composites, *ACS Nano*. 5 (2011) 3182–3190. <https://doi.org/10.1021/nn200319d>.
- 1161 [97] F. Najafi, G. Wang, S. Mukherjee, T. Cui, T. Filleter, C.V. Singh, Toughening of graphene-
 1162 based polymer nanocomposites via tuning chemical functionalization, *Compos. Sci. Technol.*
 1163 194 (2020) 108140. <https://doi.org/10.1016/j.compscitech.2020.108140>.
- 1164 [98] G. Wang, E. Gao, Z. Dai, L. Liu, Z. Xu, Z. Zhang, Degradation and recovery of
 1165 graphene/polymer interfaces under cyclic mechanical loading, *Compos. Sci. Technol.* (2017).
 1166 <https://doi.org/10.1016/j.compscitech.2017.06.004>.
- 1167 [99] G. Wang, Z. Dai, L. Liu, H. Hu, Q. Dai, Z. Zhang, Tuning the Interfacial Mechanical

- 1168 Behaviors of Monolayer Graphene/PMMA Nanocomposites, *ACS Appl. Mater. Interfaces*.
 1169 (2016). <https://doi.org/10.1021/acsami.6b03069>.
- 1170 [100] Y. Chen, Z. Dai, C. Weng, G. Wang, X. Liu, X. Cong, P. Tan, L. Liu, Z. Zhang, Engineering
 1171 the interface in mechanically responsive graphene-based films, *RSC Adv.* (2018).
 1172 <https://doi.org/10.1039/c8ra07974a>.
- 1173 [101] W. Hou, Y. Gao, J. Wang, D.J. Blackwood, S. Teo, Recent advances and future perspectives
 1174 for graphene oxide reinforced epoxy resins, *Mater. Today Commun.* 23 (2020) 100883.
 1175 <https://doi.org/10.1016/j.mtcomm.2019.100883>.
- 1176 [102] J. Feng, Z. Guo, Wettability of graphene: From influencing factors and reversible conversions
 1177 to potential applications, *Nanoscale Horizons.* 4 (2019) 526–530.
 1178 <https://doi.org/10.1039/c8nh00348c>.
- 1179 [103] N. Ojaghloou, D. Bratko, M. Salanne, M. Shafiei, A. Luzar, Solvent-Solvent Correlations across
 1180 Graphene: The Effect of Image Charges, *ACS Nano.* 14 (2020) 7987–7998.
 1181 <https://doi.org/10.1021/acsnano.9b09321>.
- 1182 [104] R. V. Dennis, L.T. Viyanalage, A. V. Gaikwad, T.K. Rout, S. Banerjee, Graphene
 1183 nanocomposite coatings for protecting lowalloy steels from corrosion, *Am. Ceram. Soc. Bull.*
 1184 (2013).
- 1185 [105] N. Mahato, M.H. Cho, Graphene integrated polyaniline nanostructured composite coating for
 1186 protecting steels from corrosion: Synthesis, characterization, and protection mechanism of the
 1187 coating material in acidic environment, *Constr. Build. Mater.* (2016).
 1188 <https://doi.org/10.1016/j.conbuildmat.2016.04.073>.
- 1189 [106] B. Ramezanzadeh, A. Ahmadi, M. Mahdavian, Enhancement of the corrosion protection
 1190 performance and cathodic delamination resistance of epoxy coating through treatment of steel
 1191 substrate by a novel nanometric sol-gel based silane composite film filled with functionalized
 1192 graphene oxide nanosheets, *Corros. Sci.* 109 (2016) 182–205.
 1193 <https://doi.org/10.1016/J.CORSCI.2016.04.004>.
- 1194 [107] K. Qi, Y. Sun, H. Duan, X. Guo, A corrosion-protective coating based on a solution-
 1195 processable polymer-grafted graphene oxide nanocomposite, *Corros. Sci.* 98 (2015) 500–506.
 1196 <https://doi.org/10.1016/J.CORSCI.2015.05.056>.
- 1197 [108] O. V. Yazyev, Y.P. Chen, Polycrystalline graphene and other two-dimensional materials, *Nat.*
 1198 *Nanotechnol.* (2014). <https://doi.org/10.1038/nnano.2014.166>.
- 1199 [109] Z. Song, V.I. Artyukhov, B.I. Yakobson, Z. Xu, Pseudo hall-petch strength reduction in
 1200 polycrystalline graphene, *Nano Lett.* (2013). <https://doi.org/10.1021/nl400542n>.
- 1201 [110] S. Mukherjee, R. Alicandri, C.V. Singh, Strength of graphene with curvilinear grain
 1202 boundaries, *Carbon N. Y.* 158 (2020) 808–817. <https://doi.org/10.1016/j.carbon.2019.11.058>.
- 1203 [111] P. Zhang, L. Ma, F. Fan, Z. Zeng, C. Peng, P.E. Loya, Z. Liu, Y. Gong, J. Zhang, X. Zhang,
 1204 P.M. Ajayan, T. Zhu, J. Lou, Fracture toughness of graphene, *Nat. Commun.* (2014).
 1205 <https://doi.org/10.1038/ncomms4782>.
- 1206 [112] A. Zandiatashbar, G.H. Lee, S.J. An, S. Lee, N. Mathew, M. Terrones, T. Hayashi, C.R. Picu,
 1207 J. Hone, N. Koratkar, Effect of defects on the intrinsic strength and stiffness of graphene, *Nat.*
 1208 *Commun.* (2014). <https://doi.org/10.1038/ncomms4186>.
- 1209 [113] Z. Dai, G. Wang, Z. Zheng, Y. Wang, S. Zhang, X. Qi, P. Tan, L. Liu, Z. Xu, Q. Li, Z. Cheng,
 1210 Z. Zhang, Mechanical responses of boron-doped monolayer graphene, *Carbon N. Y.* (2019).
 1211 <https://doi.org/10.1016/j.carbon.2019.03.014>.
- 1212 [114] A. Tiwari, R.K. Singh Raman, Durable corrosion resistance of copper due to multi-layer
 1213 graphene, *Materials (Basel)*. (2017). <https://doi.org/10.3390/ma10101112>.
- 1214 [115] T. Wu, G. Ding, H. Shen, H. Wang, L. Sun, D. Jiang, X. Xie, M. Jiang, Triggering the
 1215 continuous growth of graphene toward millimeter-sized grains, *Adv. Funct. Mater.* 23 (2013)

- 1216 198–203. <https://doi.org/10.1002/adfm.201201577>.
- 1217 [116] M. Topsakal, H. Aahin, S. Ciraci, Graphene coatings: An efficient protection from oxidation,
 1218 Phys. Rev. B - Condens. Matter Mater. Phys. 85 (2012) 155445.
 1219 <https://doi.org/10.1103/PhysRevB.85.155445>.
- 1220 [117] Y.H. Zhang, H.R. Zhang, B. Wang, Z.Y. Chen, Y.Q. Zhang, B. Wang, Y.P. Sui, B. Zhu, C.M.
 1221 Tang, X.L. Li, X.M. Xie, G.H. Yu, Z. Jin, X.Y. Liu, Role of wrinkles in the corrosion of
 1222 graphene domain-coated Cu surfaces, Appl. Phys. Lett. 104 (2014).
 1223 <https://doi.org/10.1063/1.4871000>.
- 1224 [118] J. Shang, Y. Chen, Y. Zhou, L. Liu, G. Wang, X. Li, J. Kuang, Q. Liu, Z. Dai, H. Miao, L. Zhi,
 1225 Z. Zhang, Effect of folded and crumpled morphologies of graphene oxide platelets on the
 1226 mechanical performances of polymer nanocomposites, Polymer (Guildf). 68 (2015) 131–139.
 1227 <https://doi.org/10.1016/j.polymer.2015.05.003>.
- 1228 [119] B. Vasić, A. Zurutuza, R. Gajić, Spatial variation of wear and electrical properties across
 1229 wrinkles in chemical vapour deposition graphene, Carbon N. Y. 102 (2016) 304–310.
 1230 <https://doi.org/10.1016/j.carbon.2016.02.066>.
- 1231 [120] F. Long, P. Yasaei, W. Yao, A. Salehi-Khojin, R. Shahbazian-Yassar, Anisotropic Friction of
 1232 Wrinkled Graphene Grown by Chemical Vapor Deposition, ACS Appl. Mater. Interfaces. 9
 1233 (2017) 20922–20927. <https://doi.org/10.1021/acsami.7b00711>.
- 1234 [121] Y.H. Zhang, B. Wang, H.R. Zhang, Z.Y. Chen, Y.Q. Zhang, B. Wang, Y.P. Sui, X.L. Li, X.M.
 1235 Xie, G.H. Yu, Z. Jin, X.Y. Liu, The distribution of wrinkles and their effects on the oxidation
 1236 resistance of chemical vapor deposition graphene, Carbon N. Y. 70 (2014) 81–86.
 1237 <https://doi.org/10.1016/j.carbon.2013.12.075>.
- 1238 [122] T. Qureshi, M. Ahmed, Waste Metal For Improving Concrete Performance And Utilisation As
 1239 An Alternative Of Reinforcement Bar, Int. J. Eng. Res. Appl. 5 (2015) 97–103.
- 1240 [123] T.S. Qureshi, a. Al-Tabbaa, Self-healing of drying shrinkage cracks in cement-based materials
 1241 incorporating reactive MgO, Smart Mater. Struct. 25 (2016) 084004.
 1242 <https://doi.org/10.1088/0964-1726/25/8/084004>.
- 1243 [124] S. Wu, T. Qureshi, G. Wang, Application of Graphene in Fiber-Reinforced Cementitious
 1244 Composites: A Review, Energies 2021, Vol. 14, Page 4614. 14 (2021) 4614.
 1245 <https://doi.org/10.3390/EN14154614>.
- 1246 [125] T.S. Qureshi, D.K. Panesar, B. Sidhureddy, A. Chen, P.C. Wood, Nano-cement composite
 1247 with graphene oxide produced from epigenetic graphite deposit, Compos. Part B Eng. 159
 1248 (2019). <https://doi.org/10.1016/j.compositesb.2018.09.095>.
- 1249 [126] R. Zhang, T.S. Qureshi, D.K. Panesar, Use of industrial waste in construction and a cost
 1250 analysis, Handb. Sustain. Concr. Ind. Waste Manag. (2022) 615–635.
 1251 <https://doi.org/10.1016/B978-0-12-821730-6.00019-X>.
- 1252 [127] R. Zhang, T.S. Qureshi, D.K. Panesar, Management of industrial waste and cost analysis,
 1253 Handb. Sustain. Concr. Ind. Waste Manag. (2022) 595–614. <https://doi.org/10.1016/B978-0-12-821730-6.00027-9>.
- 1255 [128] Z. Suo, Cracking and debonding of microlaminates, J. Vac. Sci. Technol. A Vacuum, Surfaces,
 1256 Film. (1993). <https://doi.org/10.1116/1.578555>.
- 1257 [129] J.W. Hutchinson, Z. Suo, Mixed Mode Cracking in Layered Materials, Adv. Appl. Mech.
 1258 (1991). [https://doi.org/10.1016/S0065-2156\(08\)70164-9](https://doi.org/10.1016/S0065-2156(08)70164-9).
- 1259 [130] M.D. Thouless, Cracking and delamination of coatings, J. Vac. Sci. Technol. A Vacuum,
 1260 Surfaces, Film. 9 (1991) 2510–2515. <https://doi.org/10.1116/1.577265>.
- 1261 [131] T. Cui, K. Yip, A. Hassan, G. Wang, X. Liu, Y. Sun, T. Filleter, Graphene fatigue through van
 1262 der Waals interactions, Sci. Adv. (2020). <https://doi.org/10.1126/sciadv.abb1335>.
- 1263 [132] O.M.E. Ylivaara, X. Liu, L. Kilpi, J. Lyytinen, D. Schneider, M. Laitinen, J. Julin, S. Ali, S.

- 1264 Sintonen, M. Berdova, E. Haimi, T. Sajavaara, H. Ronkainen, H. Lipsanen, J. Koskinen, S.P.
 1265 Hannula, R.L. Puurunen, Aluminum oxide from trimethylaluminum and water by atomic layer
 1266 deposition: The temperature dependence of residual stress, elastic modulus, hardness and
 1267 adhesion, *Thin Solid Films*. 552 (2014) 124–135. <https://doi.org/10.1016/j.tsf.2013.11.112>.
- 1268 [133] S.H. Jen, J.A. Bertrand, S.M. George, Critical tensile and compressive strains for cracking of
 1269 Al₂O₃ films grown by atomic layer deposition, *J. Appl. Phys.* 109 (2011).
 1270 <https://doi.org/10.1063/1.3567912>.
- 1271 [134] Y. Cui, S.I. Kundalwal, S. Kumar, Gas barrier performance of graphene/polymer
 1272 nanocomposites, *Carbon N. Y.* 98 (2016) 313–333.
 1273 <https://doi.org/10.1016/J.CARBON.2015.11.018>.
- 1274 [135] G. Wang, Z. Dai, Y. Wang, P. Tan, L. Liu, Z. Xu, Y. Wei, R. Huang, Z. Zhang, Measuring
 1275 interlayer shear stress in bilayer graphene, *Phys. Rev. Lett.* (2017).
 1276 <https://doi.org/10.1103/PhysRevLett.119.036101>.
- 1277 [136] G. Wang, X. Li, Y. Wang, Z. Zheng, Z. Dai, X. Qi, L. Liu, Z. Cheng, Z. Xu, P. Tan, Z. Zhang,
 1278 Interlayer Coupling Behaviors of Boron Doped Multilayer Graphene, *J. Phys. Chem. C*. 121
 1279 (2017) 26034–26043. <https://doi.org/10.1021/acs.jpcc.7b05771>.
- 1280 [137] C. Weng, G. Wang, Z. Dai, Y. Pei, L. Liu, Z. Zhang, Buckled AgNW/MXene hybrid
 1281 hierarchical sponges for high-performance electromagnetic interference shielding, *Nanoscale*.
 1282 11 (2019) 22804–22812. <https://doi.org/10.1039/c9nr07988b>.
- 1283 [138] N. Yang, T. Yang, W. Wang, H. Chen, W. Li, Polydopamine modified polyaniline-graphene
 1284 oxide composite for enhancement of corrosion resistance, *J. Hazard. Mater.* 377 (2019) 142–
 1285 151. <https://doi.org/10.1016/j.jhazmat.2019.05.063>.
- 1286 [139] Z. Zheng, L. Xiao, P. Huang, F. Wang, Polydopamine improved anticorrosion of graphene on
 1287 copper: Inhibiting galvanic corrosion and healing structure defects, *Appl. Mater. Today*. 24
 1288 (2021) 101069. <https://doi.org/10.1016/j.apmt.2021.101069>.
- 1289 [140] M. Cui, S. Ren, H. Zhao, Q. Xue, L. Wang, Polydopamine coated graphene oxide for
 1290 anticorrosive reinforcement of water-borne epoxy coating, *Chem. Eng. J.* 335 (2018) 255–266.
 1291 <https://doi.org/10.1016/J.CEJ.2017.10.172>.
- 1292 [141] X. Zhu, H. Zhao, L. Wang, Q. Xue, Bioinspired ultrathin graphene nanosheets sandwiched
 1293 between epoxy layers for high performance of anticorrosion coatings, *Chem. Eng. J.* 410
 1294 (2021) 128301. <https://doi.org/10.1016/j.cej.2020.128301>.
- 1295 [142] X. Zhu, Q. Yan, L. Cheng, H. Wu, H. Zhao, L. Wang, Self-alignment of cationic graphene
 1296 oxide nanosheets for anticorrosive reinforcement of epoxy coatings, *Chem. Eng. J.* 389 (2020)
 1297 124435. <https://doi.org/10.1016/j.cej.2020.124435>.
- 1298 [143] X. Luo, J. Zhong, Q. Zhou, S. Du, S. Yuan, Y. Liu, Cationic Reduced Graphene Oxide as Self-
 1299 Aligned Nanofiller in the Epoxy Nanocomposite Coating with Excellent Anticorrosive
 1300 Performance and Its High Antibacterial Activity, *ACS Appl. Mater. Interfaces*. 10 (2018)
 1301 18400–18415. <https://doi.org/10.1021/acsami.8b01982>.
- 1302 [144] X. Xu, Z. Zhang, J. Dong, D. Yi, J. Niu, M. Wu, L. Lin, R. Yin, M. Li, J. Zhou, S. Wang, J.
 1303 Sun, X. Duan, P. Gao, Y. Jiang, X. Wu, H. Peng, R.S. Ruoff, Z. Liu, D. Yu, E. Wang, F. Ding,
 1304 K. Liu, Ultrafast epitaxial growth of metre-sized single-crystal graphene on industrial Cu foil,
 1305 *Sci. Bull.* 62 (2017) 1074–1080. <https://doi.org/10.1016/j.scib.2017.07.005>.
- 1306 [145] W. Kong, H. Kum, S.H. Bae, J. Shim, H. Kim, L. Kong, Y. Meng, K. Wang, C. Kim, J. Kim,
 1307 Path towards graphene commercialization from lab to market, *Nat. Nanotechnol.* (2019).
 1308 <https://doi.org/10.1038/s41565-019-0555-2>.
- 1309 [146] K.C. Krogman, R.E. Cohen, P.T. Hammond, M.F. Rubner, B.N. Wang, Industrial-scale spray
 1310 layer-by-layer assembly for production of biomimetic photonic systems, *Bioinspiration and*
 1311 *Biomimetics*. (2013). <https://doi.org/10.1088/1748-3182/8/4/045005>.
- 1312 [147] H. Tang, S. Ji, L. Gong, H. Guo, G. Zhang, Tubular ceramic-based multilayer separation

- 1313 membranes using spray layer-by-layer assembly, *Polym. Chem.* (2013).
 1314 <https://doi.org/10.1039/c3py00617d>.
- 1315 [148] K. Kang, K.H. Lee, Y. Han, H. Gao, S. Xie, D.A. Muller, J. Park, Layer-by-layer assembly of
 1316 two-dimensional materials into wafer-scale heterostructures, *Nature*. (2017).
 1317 <https://doi.org/10.1038/nature23905>.
- 1318 [149] J.J. Richardson, M. Björnmalm, F. Caruso, Technology-driven layer-by-layer assembly of
 1319 nanofilms, *Science* (80-.). (2015). <https://doi.org/10.1126/science.aaa2491>.
- 1320 [150] L.H. Yang, F.C. Liu, E.H. Han, Effects of P/B on the properties of anticorrosive coatings with
 1321 different particle size, *Prog. Org. Coatings*. 53 (2005) 91–98.
 1322 <https://doi.org/10.1016/J.PORGCOAT.2005.01.003>.
- 1323 [151] RSMMeans, Construction and Cost Estimating Data, 2019. <https://www.rsmeans.com/>.
- 1324 [152] A. Younis, U. Ebead, P. Suraneni, A. Nanni, Cost effectiveness of reinforcement alternatives
 1325 for a concrete water chlorination tank, *J. Build. Eng.* 27 (2020) 100992.
 1326 <https://doi.org/10.1016/j.jobe.2019.100992>.
- 1327 [153] M. Gilles, New Development in galvanized rebar...and other maret opportunities, 2014.
 1328 <https://www.metallbulletin.com/events/download.ashx/document/speaker/7042/a0ID000000X0>
 1329 jtgMAB/Presentation.
- 1330 [154] M.M.S. Cheung, K.K.L. So, X. Zhang, Life cycle cost management of concrete structures
 1331 relative to chloride-induced reinforcement corrosion, *Struct. Infrastruct. Eng.* 8 (2012) 1136–
 1332 1150. <https://doi.org/10.1080/15732479.2010.507474>.
- 1333 [155] A.P. Kauling, A.T. Seefeldt, D.P. Pisoni, R.C. Pradeep, R. Bentini, R.V.B. Oliveira, K.S.
 1334 Novoselov, A.H. Castro Neto, The Worldwide Graphene Flake Production, *Adv. Mater.*
 1335 (2018). <https://doi.org/10.1002/adma.201803784>.
- 1336 [156] J.I. Paredes, S. Villar-Rodil, M.J. Fernández-Merino, L. Guardia, A. Martínez-Alonso, J.M.D.
 1337 Tascón, Environmentally friendly approaches toward the mass production of processable
 1338 graphene from graphite oxide, *J. Mater. Chem.* (2011). <https://doi.org/10.1039/c0jm01717e>.
- 1339 [157] C.Y. Yuan, D.A. Dornfeld, Integrated sustainability analysis of atomic layer deposition for
 1340 microelectronics manufacturing, *J. Manuf. Sci. Eng. Trans. ASME*. (2010).
 1341 <https://doi.org/10.1115/1.4001686>.
- 1342 [158] S.I. Seyed Shahabadi, J. Kong, X. Lu, Aqueous-Only, Green Route to Self-Healable, UV-
 1343 Resistant, and Electrically Conductive Polyurethane/Graphene/Lignin Nanocomposite
 1344 Coatings, *ACS Sustain. Chem. Eng.* (2017). <https://doi.org/10.1021/acssuschemeng.6b02941>.
- 1345 [159] J.L. Smith, Y.P. Virmani, Performance of Epoxy-Coated Rebars in Bridge Decks, *Fed. Highw.*
 1346 *Adm. Res. Technol.* 60 (1996) 6–12. <http://www.tfhr.gov/pubrds/fall96/p96au6.htm>.
- 1347 [160] S.R. Yeomans, Comparitive Studies of Galvanized and epoxy coated steel reinforcement in
 1348 concrete, *Spec. Publ.* 126 (1991) 355–370. <https://doi.org/10.14359/2214>.
- 1349 [161] X. Ye, J. Long, Z. Lin, H. Zhang, H. Zhu, M. Zhong, Direct laser fabrication of large-area and
 1350 patterned graphene at room temperature, *Carbon N. Y.* 68 (2014) 784–790.
 1351 <https://doi.org/10.1016/j.carbon.2013.11.069>.
- 1352 [162] S.C. Devi, R.A. Khan, Effect of Sulfate Attack and Carbonation in Graphene Oxide–
 1353 Reinforced Concrete Containing Recycled Concrete Aggregate, *J. Mater. Civ. Eng.* 32 (2020)
 1354 04020339. [https://doi.org/10.1061/\(ASCE\)MT.1943-5533.0003415](https://doi.org/10.1061/(ASCE)MT.1943-5533.0003415).
- 1355 [163] X. Li, T. Yang, Y. Yang, J. Zhu, L. Li, F.E. Alam, X. Li, K. Wang, H. Cheng, C. Te Lin, Y.
 1356 Fang, H. Zhu, Large-Area Ultrathin Graphene Films by Single-Step Marangoni Self-Assembly
 1357 for Highly Sensitive Strain Sensing Application, *Adv. Funct. Mater.* 26 (2016) 1322–1329.
 1358 <https://doi.org/10.1002/adfm.201504717>.
- 1359 [164] C. Chen, G. Xiao, Y. He, F. Zhong, H. Li, Y. Wu, J. Chen, Bio-inspired superior barrier self-
 1360 healing coating: Self-assemble of graphene oxide and polydopamine-coated halloysite

1361 nanotubes for enhancing corrosion resistance of waterborne epoxy coating, *Prog. Org.*
1362 *Coatings.* (2019). <https://doi.org/10.1016/j.porgcoat.2019.105402>.

1363 [165] G. Cui, C. Zhang, A. Wang, X. Zhou, X. Xing, J. Liu, Z. Li, Q. Chen, Q. Lu, Research
1364 progress on self-healing polymer/graphene anticorrosion coatings, *Prog. Org. Coatings.* 155
1365 (2021). <https://doi.org/10.1016/j.porgcoat.2021.106231>.

1366 [166] T. Qureshi, A. Al-Tabbaa, *Self-Healing Concrete and Cementitious Materials*, in: *Adv. Funct.*
1367 *Mater.*, 2020. <https://doi.org/10.5772/intechopen.92349>.

1368 [167] H.M. Yamamoto, M. Nakano, M. Suda, Y. Iwasa, M. Kawasaki, R. Kato, A strained organic
1369 field-effect transistor with a gate-tunable superconducting channel, *Nat. Commun.* 4 (2013).
1370 <https://doi.org/10.1038/ncomms3379>.

1371 [168] G. Chilkoor, K. Jawaharraj, B. Vemuri, A. Kutana, M. Tripathi, D. Kota, T. Arif, T. Filleter,
1372 A.B. Dalton, B.I. Jakobson, M. Meyyappan, M.M. Rahman, P.M. Ajayan, V. Gadhamshetty,
1373 Hexagonal boron nitride for sulfur corrosion inhibition, *ACS Nano.* 14 (2020) 14809–14819.
1374 <https://doi.org/10.1021/acsnano.0c03625>.

1375 [169] A. Nawaz, S. Goudarzi, M.A. Asghari, S. Pichiah, G.S. Selopal, F. Rosei, Z.M. Wang, H.
1376 Zarrin, Review of Hybrid 1D/2D Photocatalysts for Light-Harvesting Applications, *ACS Appl.*
1377 *Nano Mater.* 4 (2021) 11323–11352. <https://doi.org/10.1021/acsanm.1c01014>.

1378 [170] V. Sajith, K. Vidya, L. Jonghoon, V. Vikas, Y. Sadegh, S. Jianfeng, K. Suppanat, V. Soumya,
1379 V. Robert, K.R. Ajit, T. Chandra Sekhar, P.M. Ajayan, 2D Heterostructure coatings of h BN-
1380 MoS 2 layers for corrosion resistance, *J. Phys. D. Appl. Phys.* 50 (2017) 45301.
1381 <http://stacks.iop.org/0022-3727/50/i=4/a=045301>.

1382 [171] S. Susarla, G. Chilkoor, J.R. Kalimuthu, M.A.S.R. Saadi, Y. Cui, T. Arif, T. Tsafack, A.B.
1383 Puthirath, P. Sigdel, B. Jasthi, P.M. Sudeep, L. Hu, A. Hassan, S. Castro-Pardo, M. Barnes, S.
1384 Roy, R. Verduzco, M.G. Kibria, T. Filleter, H. Lin, S.D. Solares, N. Koratkar, V.
1385 Gadhamshetty, M.M. Rahman, P.M. Ajayan, Corrosion Resistance of Sulfur–Selenium Alloy
1386 Coatings, *Adv. Mater.* 33 (2021). <https://doi.org/10.1002/adma.202104467>.

1387